Martiskainen *et al.*
Molecular Neurodegeneration (2025) 20:50
https://doi.org/10.1186/s13024-025-00830-3

Molecular Neurodegeneration

RESEARCH ARTICLE

Open Access

Monoallelic *TYROBP* deletion is a novel risk factor for Alzheimer's disease

Henna Martiskainen[1*†], Roosa-Maria Willman[1†], Päivi Harju[1], Sami Heikkinen[1], Mette Heiskanen[1], Stephan A. Müller[2,3], Rosa Sinisalo[1], Mari Takalo[1], Petra Mäkinen[1], Teemu Kuulasmaa[1], Viivi Pekkala[4], Ana Galván del Rey[1], Sini-Pauliina Juopperi[1], Heli Jeskanen[1], Inka Kervinen[1], Kirsi Saastamoinen[1], FinnGen, Marja Niiranen[5], Sami V. Heikkinen[6], Mitja I. Kurki[7,8,9,10], Jarkko Marttila[11], Petri I. Mäkinen[4], Hannah Rostalski[4], Tomi Hietanen[4], Tiia Ngandu[12,13], Jenni Lehtisalo[6,12], Céline Bellenguez[14], Jean-Charles Lambert[14], Christian Haass[2,15,16], Juha Rinne[17,18], Juhana Hakumäki[11,19], Tuomas Rauramaa[20,21], Johanna Krüger[22,23,24], Hilkka Soininen[6], Annakaisa Haapasalo[4], Stefan F. Lichtenthaler[2,3,16], Ville Leinonen[25,26], Eino Solje[5,26] and Mikko Hiltunen[1*]

Abstract

Biallelic loss-of-function variants in *TYROBP* and *TREM2* cause autosomal recessive presenile dementia with bone cysts known as Nasu-Hakola disease (NHD, alternatively polycystic lipomembranous osteodysplasia with sclerosing leukoencephalopathy, PLOSL). Some other *TREM2* variants contribute to the risk of Alzheimer's disease (AD) and frontotemporal dementia, while deleterious *TYROBP* variants are globally extremely rare and their role in neurodegenerative diseases remains unclear. The population history of Finns has favored the enrichment of deleterious founder mutations, including a 5.2 kb deletion encompassing exons 1–4 of *TYROBP* and causing NHD in homozygous carriers. We used here a proxy marker to identify monoallelic *TYROBP* deletion carriers in the Finnish biobank study FinnGen combining genome and health registry data of 520,210 Finns. We show that monoallelic *TYROBP* deletion associates with an increased risk and earlier onset age of AD and dementia when compared to noncarriers. In addition, we present the first reported case of a monoallelic *TYROBP* deletion carrier with NHD-type bone cysts. Mechanistically, monoallelic *TYROBP* deletion leads to decreased levels of DAP12 protein (encoded by *TYROBP*) in myeloid cells. Using transcriptomic and proteomic analyses of human monocyte-derived microglia-like cells, we show that upon lipopolysaccharide stimulation monoallelic *TYROBP* deletion leads to the upregulation of the inflammatory response and downregulation of the unfolded protein response when compared to cells with two functional copies of *TYROBP*. Collectively, our findings indicate *TYROBP* deletion as a novel risk factor for AD and suggest specific pathways for therapeutic targeting.

Keywords Alzheimer's disease, DAP12, Genetics, Nasu-Hakola disease, Polycystic lipomembranous osteodysplasia with sclerosing leukoencephalopathy, TYROBP

†Henna Martiskainen and Roosa-Maria Willman contributed equally to this work.

*Correspondence:
Henna Martiskainen
henna.martiskainen@uef.fi
Mikko Hiltunen
mikko.hiltunen@uef.fi
Full list of author information is available at the end of the article

Background

The TYRO protein tyrosine kinase-binding protein (*TYROBP*) gene encodes for DAP12 that functions as a transmembrane signaling adapter in immune cells of the myeloid lineage. Within the brain, DAP12 is expressed by microglia, where it mediates intracellular signaling from various cell surface receptors including TREM2, CR3, and SIRP1β. DAP12 has been identified as a central microglial hub in networks regulating Alzheimer's disease (AD) pathology and microglial surveillance functions [1, 2].

Genetic associations with different neurodegenerative diseases highlight the indispensable role of TREM2-DAP12 signaling in brain health. Biallelic (both alleles carry a variant, homozygous or compound heterozygous) loss-of-function variants in either *TYROBP* or *TREM2* cause Nasu-Hakola disease (NHD) known also as polycystic lipomembranous osteodysplasia with sclerosing leukoencephalopathy (PLOSL). NHD is a rare recessive neurodegenerative disorder characterized by bone cysts and pathological fractures at early adulthood, followed by early-onset frontotemporal type dementia and death at the middle age [3, 4]. Additionally, biallelic *TREM2* variants contribute to recessively inherited early-onset behavioral variant frontotemporal dementia with white matter abnormalities but without bone involvement [5–7], while monoallelic missense variants in *TREM2* significantly increase the risk of AD [8, 9]. Despite the close functional connection between TREM2 and DAP12, the potential contribution of *TYROBP* variants to neurodegenerative diseases remain inconclusive [10–12]. One possible explanation for this disparity could be the extreme rarity of potentially deleterious *TYROBP* variants across most of the studied populations.

The Finnish population, characterized by a unique history of relative isolation and population bottlenecks followed by rapid expansion, harbors a relatively homogeneous genetic background with a small number of deleterious variants at higher frequencies than is commonly observed in other populations. Notably, among the deleterious founder mutations enriched in the Finnish population is a 5.2-kb deletion covering four of the five exons of *TYROBP* and causing NHD in homozygous carriers [3, 13]. Based on the prevalence of NHD in Finland (1:500,000–1:1,000,000) [13] and a previous study [11], the frequency of monoallelic *TYROBP* deletion carriers is estimated to be around 1:300–1:500. One previous study has explored the possibility that the Finnish *TYROBP* deletion might be a risk factor for neurodegenerative diseases in the monoallelic carriers but found no association [11]. However, the result may be considered inconclusive due to the limited number of identified *TYROBP* deletion carriers [11]. Studies in larger cohorts have been hindered by the difficulty to detect large structural variants in generally used genotyping array data, which mostly comprises single nucleotide variants (SNVs).

We hypothesized that assessing *TYROBP* deletion in FinnGen, a large, well-characterized biobank-scale cohort representing 10% of the Finnish population [14], would provide a more comprehensive understanding on the potential phenotype effect of the monoallelic *TYROBP* deletion and, more broadly, on the effect of partial *TYROBP* loss. The feasibility of FinnGen for such analyses was recently demonstrated by a study that identified novel significant phenotype associations in the monoallelic state for many known recessive disease-causing variants [15].

In the present study, we identified two SNVs as genetic proxies for the Finnish *TYROBP* deletion and confirmed that this deletion is a Finnish founder mutation. Importantly, our findings revealed that the Finnish *TYROBP* deletion associates with an increased risk and earlier onset of dementia and AD in the monoallelic carriers. Furthermore, we present a case of monoallelic *TYROBP* deletion carrier exhibiting cystic bone lesions reminiscent of those detected in NHD patients, but without cognitive symptoms. Finally, we demonstrated that mono- and biallelic *TYROBP* deletion induces functional alterations in microglia-like cells in vitro.

Methods

Study design

The overall aim of our study was to assess the phenotypic and functional effects of a Finnish founder mutation, 5.2 kb *TYROBP* deletion, that is known to cause the early-onset neurodegenerative disease NHD in biallelic state. We hypothesized that the monoallelic *TYROBP* deletion may be a risk factor for neurodegeneration later in life and may induce functional changes in the microglial cells. In the first part of the study, we aimed to elucidate the clinical phenotype of the monoallelic *TYROBP* deletion in a large, well-characterized biobank cohort FinnGen. To achieve this aim, we first identified the founder haplotype and genetic proxy markers for the Finnish *TYROBP* deletion by utilizing whole genome sequencing (WGS) of three Finnish NHD patients. Using the proxy markers, we conducted phenome-wide association study in FinnGen data freeze 12 (DF12) which contains genome and digital healthcare data on 520,210 Finnish individuals and 2,489 clinical endpoints. To complement the picture of clinical phenotype induced by *TYROBP* deletion, we present case reports of two monoallelic *TYROBP* deletion carriers. The first case is a 34-year-old female presenting classic NHD bone cysts in wrists and ankles. The second case is a 75-year-old female diagnosed with idiopathic normal pressure hydrocephalus (iNPH), with

amyloid β (Aβ)-positive frontal cortical brain biopsy and cerebrospinal fluid (CSF) biomarker profile indicative of AD-related brain pathology.

In the second part of the study, we aimed to experimentally evaluate the effects of *TYROBP* deletion using microglia-like models in vitro. Human monocytes for monocyte-derived microglia-like cell (MDMi) differentiation were extracted from peripheral venous blood samples obtained from carriers of the Finnish *TYROBP* deletion (> 60 years), non-carrier age-matched controls, and NHD patients (30–40 years). MDMi cultures in basal conditions or after treatment with myelin or lipopolysaccharide (LPS) were used for omics and targeted functional analyses as detailed below. To study the effect of *TYROBP* loss-of-function on M-CSF induced signaling, we created *Tyrobp* knock-out (KO) mouse microglial BV2 cell lines using CRISPR-Cas9 genome editing and clonal selection or used siRNA to partially silence *Tyrobp* (Additional file 1, Supplementary Materials and Methods).

All study protocols concerning human samples were approved by Medical Research Ethics Committee of Wellbeing Services County of North Savo. Written informed consent was obtained from all participants. The Ethics Committee of the Hospital District of Helsinki and Uusimaa (HUS) has coordinated the approval for FinnGen Study.

Study subjects

NHD patients, monoallelic *TYROBP* deletion carriers, and unrelated controls were recruited during 2020–2024 from Neurology clinics at Kuopio University Hospital and Oulu University Hospital, Kuopio University Hospital NPH registry [16], Finnish Geriatric Intervention Study to Prevent Cognitive Decline and Disability (FINGER) [17], Biobank of Eastern Finland, and Auria Biobank. Blood samples for monocyte and/or DNA isolation were collected following written informed consent from each participant.

The FinnGen Study (https://www.finngen.fi/en) is a large biobank-scale research project which combines genome data with digital healthcare data based on national health registers [14]. FinnGen includes samples collected by the Finnish biobanks as well as legacy samples from previous research cohorts that have been transferred to the biobanks. FinnGen Study approved the use of the data in the present work.

The study subjects in FinnGen have provided informed consent for biobank research based on the Finnish Biobank Act. Alternatively, separate research cohorts that were collected prior to the Finnish Biobank Act coming into effect (September 2013) and start of FinnGen (August 2017), were collected based on study-specific consents and later transferred to the Finnish biobanks after approval by the Finnish Medicines Agency Fimea. Participant recruitment followed the biobank protocols approved by Fimea. The Coordinating Ethics Committee of the Hospital District of Helsinki and Uusimaa (HUS) statement number for the FinnGen study is HUS/990/2017. The complete list of ethics committee approval numbers, study permits, and biobank sample and data accession numbers are included in the Declarations at the end of the manuscript.

Genotyping

For non-FinnGen study participants, genomic DNA was extracted from peripheral whole blood using QIAamp DNA Blood Mini Kit (Qiagen, Hilden, Germany). DNA for a subset of 50 imputed *TYROBP* deletion proxy marker carriers from the FinnGen cohort was obtained through the Biobank of Eastern Finland.

Library preparation and WGS on Illumina NovaSeq sequencing platform was carried out at Novogene (Novogene (UK) Company Limited, Cambridge, UK). WGS data were initially processed using the nf-core sarek pipeline (release 3.1) with default settings [18], and the GATK GRCh38 as the reference genome. After identifying potential problems in the initial read alignment at and near the deletion breakpoints, WGS data were aligned again to the human reference genome (GRCh38) using a splice-aware aligner STAR (v2.7.9a) [19] with essential non-default settings: –outFilterMultimapNmax 1, –outFilterMismatchNmax 3, –alignIntronMax 10,000 and –alignMatesGapMax 10,000.

TYROBP deletion-specific PCR was carried out as described previously [11]. Genotyping of SNV 19:35,901,079-T-G was carried out by Sanger sequencing. In brief, the target region was amplified by PCR using primers 5'- GCGAACGCAGTCCCTGAATGG- 3' (forward) and 5'-CCTCCCTCTGGACCCAGTAA- 3' (reverse) and the PCR product was cleaned using NucleoSpin Gel and PCR Clean-up mini kit (Macherey–Nagel, Düren, Germany). The purified PCR product was combined with the reverse primer and sent to Macrogen Europe (Amsterdam, the Netherlands) for Sanger sequencing. Sanger sequencing was reliable only from reverse direction due to the presence of several poly-T repeats between the forward primer and the variant. *APOE* genotyping was carried out with pre-designed TaqMan SNP genotyping assays for rs429358 and rs7412 (both from ThermoFisher Scientific). TaqMan SNP genotyping assays were performed according to manufacturer's instructions, and all samples were assayed in duplicate.

The whole FinnGen cohort has been genotyped with multiple Illumina (Illumina Inc., San Diego, USA) and

Affymetrix (Thermo Fisher Scientific, Santa Clara, CA, USA) chip arrays as part of the FinnGen Study. Chip genotype data were imputed using the Finnish population-specific imputation reference panel Sequencing Initiative Suomi project (SISu v4.2), Institute for Molecular Medicine Finland (FIMM), University of Helsinki, Finland (http://sisuproject.fi).

FinnGen analyses

Phenotype information and clinical endpoints in FinnGen are based on different national health registries, including hospital discharge registers, prescription medication purchase registers, and cancer registers. A complete list of FinnGen endpoints and their respective controls are available at https://www.finngen.fi/en/researchers/clinical-endpoints and can be explored at https://risteys.finngen.fi/.

In this study we used summary statistics and data from the FinnGen data release R12. GWAS studies for FinnGen core endpoints were performed with REGENIE 2.2.4. A detailed description of the analytical methods is available at https://github.com/FINNGEN/regenie-pipelines. Phenotype associations for variant rs1244787406-G across 2489 FinnGen core analysis endpoints were visualized using LAVAA [20]. Regional association plots for the endpoint 'dementia including primary care registry' were generated with topr 2.0.0 package in R 4.3.2 [21, 22]. Linkage disequilibrium in-sample dosage in the *TYROBP*-locus (3 Mb window around the lead variant) in FinnGen was computed using LDstore2 [23] and fine-mapping was carried out using SuSiE [24] with the maximum number of causal variants in a locus L = 10.

The map visualizing the regional allele frequency of rs1244787406-G was created in R based on the region of birth for minor and major allele carriers. Kaplan–Meier curves were drawn in R using package survminer v0.4.9 [25].

Radiological imaging

The monoallelic *TYROBP* deletion carrier and the NHD patient were imaged as part of diagnostic procedure with conventional x-rays (Siemens Ysio Max, Erlangen, Germany) for skeletal features of the hands and feet, and at 3,0 Tesla MRI (Philips Achieva, Best, NL) and 1,5 Tesla MRI (GE Signa Artist, Milwaukee, USA) with standard clinical sequences, including T1, T2, FLAIR, DWI, and susceptibility weighted imaging, for potential brain pathology. The 3D T1 MRI data were also analyzed by brain volumetry software, cNeuro (Combinostics Ltd, Tampere, Finland).

Immunohistochemistry and CSF biomarkers

Diagnostic brain biopsy specimen collected during NPH shunt surgery were used for immunohistochemical analysis. Immunostaining for Iba-1 and Aβ was performed as described previously [26]. Full section brightfield images were obtained with Hamamatsu NanoZoomer-XR Digital slide scanner with 20x (NA 0.75) objective (Hamamatsu Photonics K.K., Shizuoka, Japan) and analyzed as described previously [26]. In short, Aβ plaques were manually outlined in NDP.view2 software (Hamamatsu Photonics K.K.) to obtain the plaque size. The plaque-associated microglia with clearly visible soma were manually counted by an investigator blinded to sample identity.

CSF samples from the same NPH patients were obtained by lumbar puncture. Levels of AD-related biomarkers $A\beta_{42}$, total Tau (T-Tau), and Tau phosphorylated at Serine 181 (P-Tau 181) were analyzed using a commercial enzyme-linked immunosorbent assay (Innotest, Fujirebio, Ghent, Belgium).

Monocyte isolation and MDMi differentiation

To extract peripheral blood mononuclear cells (PBMCs), 60–100 ml peripheral venous blood was collected from participants and processed within 24 h of sample collection. PBMCs were extracted by density gradient centrifugation over Ficoll-Paque PLUS (#17–1440 -02, Cytiva, Marlborough, MA, USA) in SepMate- 50 tubes (#85,450 Stemcell Technologies, Vancouver, Canada). PBMC were either cryoprotected in CryoStor CS10 (Stemcell Technologies) or used directly for CD14-positive monocyte isolation using human CD14 MicroBeads (Miltenyi Biotec, Bergisch Gladbach, Germany) and magnetic-activated cell sorting. When using cryopreserved PBMCs, the cells were thawed at 37 °C for 5 min, washed in RPMI medium containing 20% FBS and incubated for 30 min at 37 °C in RPMI/20% FBS to allow the cells to recover from the thawing prior to monocyte isolation.

To differentiate monocytes into MDMi, monocytes were plated at 0.5×10^6 cells per well in 12-well plates (for RNA-sequencing, LC–MS/MS, and alphaLISA) or in 96-well plates at 1×10^5 cells per well (for conditioned medium). Monocyte differentiation into MDMis was done according to a previously published protocol [27], by culturing the monocytes for 10–12 days in vitro (DIV) under standard humidified environment (+ 37 °C, 5% CO2) in MDMi culture medium consisting of RPMI- 1640 Glutamax (#61,870,036, Gibco, Billings, MT, USA) supplemented with 1% penicillin/streptomycin and a mixture of the following human recombinant cytokines: M-CSF (10 ng/ml, #574,804, Biolegend, San Diego, CA, USA), GM-CSF (10 ng/ml, #215-GM- 010/

CF, R&D Systems, Minneapolis, MN, USA), NGF-β (10 ng/ml, #256-GF- 100, R&D Systems), CCL2 (100 ng/ml, #571,404, Biolegend), and IL- 34 (100 ng/ml, #5265-IL-010/CF, R&D Systems).

RNA extraction and RNA-sequencing

After MDMi differentiation, conditioned medium was replaced with fresh MDMi culture medium or with culture medium containing myelin (25 µg/ml) or LPS (200 ng/ml, O26:B6, L5543, Sigma Aldrich), and the cells were cultured for 24 h prior to sample collection. For total RNA extraction, cells from 2–3 replicate wells/donor were collected into ice-cold PBS and RNA was extracted immediately. Acutely isolated monocytes were placed in Macherey–Nagel™ NucleoProtect RNA reagent (ThermoFisher Scientific) and stored at +4 °C until RNA extraction. RNA was isolated using High Pure RNA Isolation Kit (11,828,665,001, Roche), and the RNA extracts were stored at − 80 °C until further use. Culture preparation and RNA sequencing of induced pluripotent stem cell (iPSC) and iPSC-derived microglia (iMG) has been described earlier [28].

Library preparation and RNA sequencing was conducted by Novogene (UK) Company Limited. In brief, mRNA enrichment was performed with oligo(dT) bead pulldown, from where the pulldown material was subjected to fragmentation, followed by reverse transcription, second strand synthesis, A-tailing, and sequencing adaptor ligation. The final amplified and size selected library comprised 250–300-bp insert cDNA and paired-end 150 bp sequencing was executed with an Illumina high-throughput sequencing platform. Sequencing yielded 4.4–26.9 million sequenced fragments per sample.

The 150 nucleotide pair-end RNA-seq reads were quality-controlled using FastQC (version 0.11.7) (https://www.bioinformatics.babraham.ac.uk/projects/fastqc/). Reads were then trimmed with Trimmomatic (version 0.39) [29] to remove Illumina sequencing adapters and poor quality read ends, using as essential settings: ILLUMINACLIP:2:30:10:2:true, SLIDINGWINDOW:4:10, LEADING:3, TRAILING:3, MINLEN:50. Trimmed reads were aligned to the Gencode human transcriptome version 38 (for genome version hg38) using STAR (version 2.7.9a) [19] with essential non-default settings: –seedSearchStartLmax 12, –alignSJoverhangMin 15, –outFilterMultimapNmax 100, –outFilterMismatchNmax 33, –outFilterMatchNminOverLread 0, –outFilterScoreMinOverLread 0.3, and –outFilterType BySJout. The unstranded, uniquely mapping, gene-wise counts for primary alignments produced by STAR were collected in R (version 4.2.2) using Rsubread::featureCounts (version 2.12.3) [30], ranging from 3.3 to 22.1 million per sample. Differentially expressed genes (DEGs) between experimental groups were identified in R (version 4.2.0) using DESeq2 (version 1.36.0) [31] by employing Wald statistic and lfcShrink for FC shrinkage (type = "apeglm") [32]. Comparisons between *TYROBP* genotype groups were performed adjusting for the *APOE* ε genotype, and between monocytes and MDMi cells by adjusting for donor (equivalent of paired test). Pathway enrichment analysis was performed on the gene lists ranked by the pairwise DEG test log2 FCs in R using clusterProfiler::GSEA (version 4.4.4) [33] with Molecular Signatures Database gene sets (MSigDB, version 2022.1) [34].

Proteomics analysis

MDMi were cultured and treated as described above for RNA-sequencing. Cultured MDMi were lysed in RIPA lysis buffer (50 mM Tris–Cl, 150 mM NaCl, 1% NP- 40, 0.05% sodium deoxycholate, 0.01% SDS, pH 7.5) by incubation on ice for 20 min with intermediate vortexing. Cell debris and undissolved material were removed by centrifugation at 16.000 × g for 10 min at 4 °C, and protein concentration was determined using a BCA Assay (Thermo Fisher Scientific). 10 µg of each sample were diluted 1:2 in water and benzonase (Sigma-Aldrich) digestion was performed with 10 units for 30 min at 37 °C to remove remaining DNA/RNA. Protein digestion was performed with 125 ng LysC and 125 µg trypsin (Promega) using the single-pot solid-phase enhanced sample preparation (SP3) [35]. The peptide solution was filtered through 0.22 µm Costar SPIN-X columns (Corning) and dried by vacuum centrifugation. Samples were dissolved in 20 µL 0.1% formic acid using a sonication batch (Hielscher) and the peptide concentration was measured using the Qubit protein assay (Thermo Fisher Scientific).

An amount of 350 ng of peptides were separated on an in-house packed C18 analytical column (15 cm × 75 µm ID, ReproSil-Pur 120 C18-AQ, 1.9 µm, Dr. Maisch GmbH) using a binary gradient of water and acetonitrile (B) containing 0.1% formic acid at flow rate of 300 nL/min (0 min, 2% B; 2 min, 5% B; 70 min, 24% B; 85 min, 35% B; 90 min, 60% B) and a column temperature of 50 °C. A Data Independent Acquisition Parallel Accumulation–Serial Fragmentation (DIA-PASEF) method with a cycle time of 1.4 s was used for spectrum acquisition. Briefly, ion accumulation and separation using Trapped Ion Mobility Spectrometry (TIMS) was set to a ramp time of 100 ms. One scan cycle included one TIMS full MS scan and The DIA-PASEF windows covered the m/z range from 350–1,000 m/z with 26 windows of 27 m/z with an overlap of 1 m/z. The raw data was analyzed using the software DIA-NN version 1.8 [36] for protein label-free quantification (LFQ). A one protein per gene

canonical fasta database of Homo Sapiens (download date March 1 st 2023, 20,603 entries) from UniProt and a fasta database with 246 common potential contaminations from Maxquant [37] were used to generate a spectral library in DIA-NN with a library free search which included 10,615 proteins. Trypsin was defined as protease. Two missed cleavages were allowed, and peptide charge states were set to 2–4. Carbamidomethylation of cysteine was defined as static modification. Acetylation of the protein N-term as well as oxidation of methionine were set as variable modifications. The false discovery rate for both peptides and proteins was adjusted to less than 1%. Data normalization was disabled.

Identification of differentially expressed, *APOE* ε genotype-corrected proteins between experimental groups, non-normalized LFQ intensities as the starting point, and the subsequent pathway enrichment were done as for the RNA-seq data, except using version 4.2.3 for R and version 1.38.3 for DESeq2 [31].

AlphaLISA

CD14 + monocytes were isolated from PBMC as described above and lysed in AlphaLISA lysis buffer. MDMi were prepared from monocytes as described above and lysed in AlphaLISA lysis buffer. The lysates were stored at − 20 °C until measured.

Total DAP12 levels were measured from the cell lysates using AlphaLISA Surefire Ultra Total DAP12 Detection Kit (ALSU-TDAP12-A-HV, Revvity), and the results were normalized to GAPDH levels measured from the same lysate using AlphaLISA Surefire Ultra Human and Mouse Total GAPDH Detection Kit (ALSU-TGAPD-B-HV, Revvity). Samples were measured as duplicates.

Cytokine measurement in conditioned medium

MDMi were treated with 200 ng/ml LPS for 24 h. Conditioned medium was collected, centrifuged at 5,000 × *g* at + 4 °C for 10 min, supplemented with protease inhibitor, and stored at − 80 °C. IL- 1β, IL- 6, and IL- 10 were measured using a custom U-plex assay (Meso Scale Diagnostics, Rockville, MD, USA). A phase contrast image was captured before the LPS treatment on IncuCyte S3, and the data were normalized to cell confluency. TNFα was measured from the conditioned medium using commercial ELISA kit (88–7346 - 22, Thermo Fisher) according to manufacturer's instructions. Data is shown as average of three replicate wells/donor measured in duplicates.

Myelin isolation

Myelin was isolated from adult male C57BL/6 J mice using the sucrose gradient protocol described elsewhere [38, 39]. 0.85 M and 0.32 M sucrose solutions were used for the gradient and Beckman Ultracentrifuge with Ti 50.2 rotor for the centrifugation. The concentration of the myelin preparation was determined using Pierce BCA Protein Assay kit (23,225, Thermo Scientific) and stored at − 80 °C until used.

Statistical analysis

Statistical analyses and data visualization were performed in R 4.3.2 [22] and GraphPad Prism v10. Chi-squared test was used to analyze regional allele frequency. Survival analysis comparing disease-free survival of rs1244787406-G carriers and noncarriers was performed in R where Kaplan–Meier curves were drawn using package survminer v0.4.9 [25] and cox proportional hazards model was performed with package survival v3.2–7 [40, 41]. Independent samples T-test was used to analyze normally distributed immunohistochemistry and CSF biomarker data between the *APOE* ε3ε3 and ε3ε4 groups and cytokine data between monoallelic *TYROBP* deletion carriers and noncarriers. Additional information on the statistical test, sample size, and technical replicates is given in the figure legends.

Results

Intronic SNVs in *TYROBP* and *NFKBID* are proxy markers for the Finnish *TYROBP* deletion

To identify genetic proxy markers for the Finnish *TYROBP* deletion, we performed WGS analysis on three NHD patients unrelated up to at least 3rd degree. WGS confirmed biallelic deletion spanning approx. 5.2 kb and encompassing the exons 1–4 of *TYROBP* in all three NHD patients (Fig. 1A).

The haplotype containing the Finnish *TYROBP* deletion shared by all Finnish NHD patients has been shown to cover at least 68.915 kb immediately upstream of the deletion (Fig. 1B) [3, 13]. We focused our search of *TYROBP* deletion-associated single nucleotide variants (SNVs) to this shared haplotype region, even though the shared area of homozygosity in the NHD patients included in our study was considerably larger, at least 1.95 Mb, spanning both up- and downstream of the deletion. A total of seven SNVs homozygous for the minor allele in the NHD patients were detected in the shared haplotype region (Table 1). All the identified variants were intronic or intergenic with minor allele frequency (MAF) of 0.0031–0.79 in the Finnish population [42]. Interestingly, the two variants closest to the deletion, rs1002399693 (19:35,905,673 G > C in *TYROBP* intron 4, MAF = 0.0032) and rs1244787406 (19:35,901,079 T > G in *NFKBID* intron 1, MAF = 0.0031) were enriched in the Finnish population compared to non-Finnish Europeans, and had MAF matching the estimated carrier frequency of the Finnish 5.2-kb *TYROBP* deletion [11].

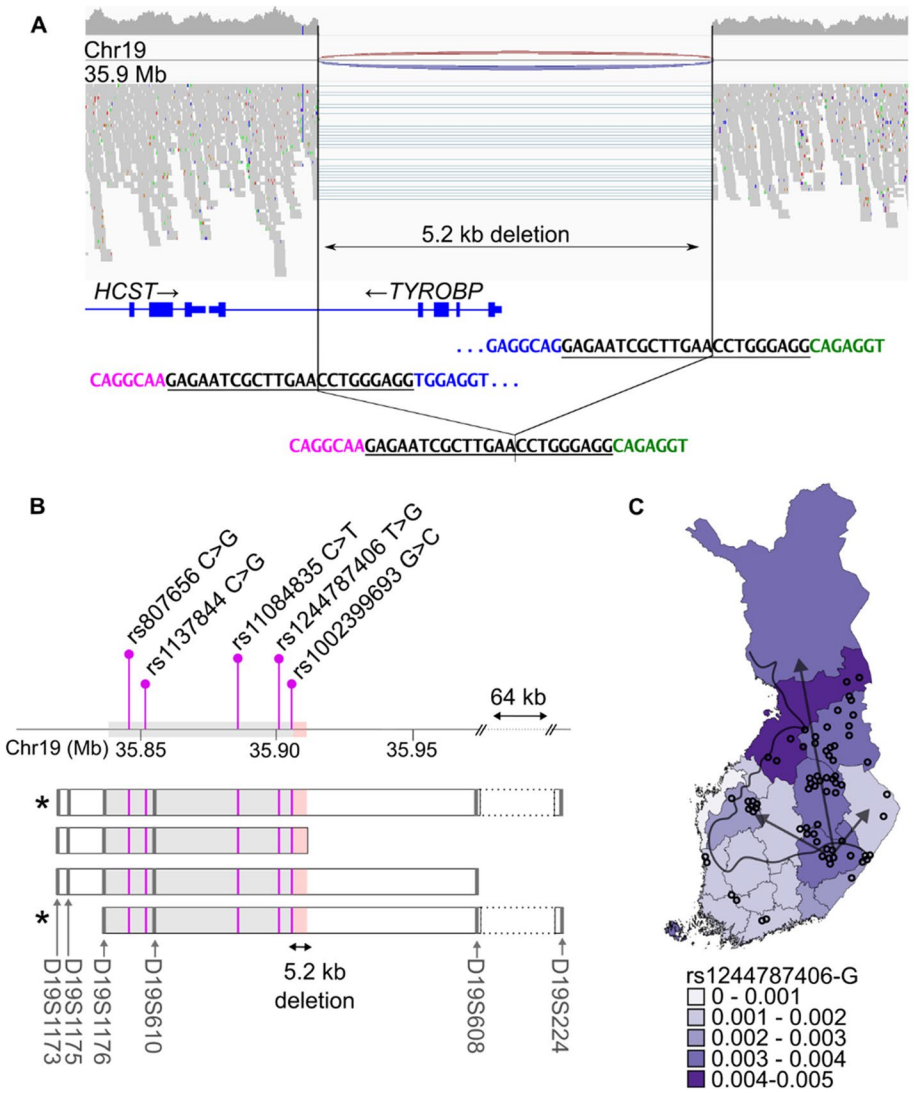

Fig. 1 The Finnish 5.2 kb *TYROBP* deletion. **A** WGS data show homozygous 5.2-kb deletion encompassing *TYROBP* exons 1–4 in a Finnish NHD patient. The horizontal lines indicate WGS reads spanning across the deletion. The deletion breakpoints are located within a 23-bp identical sequence (black, underlined). **B** Schematic of the *TYROBP* deletion founder haplotype. The boxes indicate haplotype blocks identified using microsatellite markers (grey bars) [13]. The grey shading indicates the haplotype region shared by all Finnish NHD patients, while the red shading indicates the 5.2-kb *TYROBP* deletion. Asterisks denote the haplotypes detected in the NHD patients in the current study. Purple lines indicate the SNVs identified in the current study within the shared haplotype region. **C** Regional allele frequency of rs1244787406-G in Finland. The black line separates the early settlement region along the southern and western coastlines from the late settlement region that was permanently inhabited from the sixteenth century onwards by internal migration (arrows) mainly from the current South Savo region in the southeastern Finland. The circles represent the birth places of the grandparents of the Finnish NHD patients according to [43]. The highest present day allele frequencies of the *TYROBP* deletion proxy marker rs1244787406-G are detected in the late settlement area and coincide with the previously reported regional enrichment

Next, we explored the *TYROBP* deletion haplotype and individual SNVs in the FinnGen data. Two variants were not available in FinnGen, and thus, haplotype based on imputed, phased genotypes of five SNVs was used to identify putative *TYROBP* deletion carriers. Among the 520,210 individuals, the haplotype consisting of five SNVs identified 2,231 putative *TYROBP* deletion carriers, corresponding to MAF = 0.0021. All the same 2,231 individuals and one additional individual were identified when using only the SNV rs1244787406 T > G or rs1002399693 G > C, suggesting that either of these SNVs alone could be used as a proxy marker for the 5.2-kb *TYROBP* deletion. Since the imputation Info score for these variants in FinnGen is only 0.84, we confirmed

Table 1 The 5.2 kb *TYROBP* deletion-associated haplotype identified based on WGS

rsID	Location (GRCh38)	Alleles, Ref > Alt	FinnGen r12		gnomAD v4.0.0		
			MAF	INFO	MAF Finnish	MAF NFE	Finnish enrichment
rs12462044	19:35,837,074	A > G	NA	NA	0.096	0.081	1.19
rs12462535	19:35,837,076	T > A	NA	NA	0.11	0.094	1.17
rs807656	**19:35,847,275**	**C > G**	**0.78**	**0.97**	**0.79**	**0.72**	**1.10**
rs1137844	**19:35,852,177**	**C > G**	**0.38**	**0.98**	**0.38**	**0.31**	**1.23**
rs11084835	**19:35,886,985**	**C > T**	**0.32**	**0.98**	**0.32**	**0.3**	**1.07**
rs1244787406	**19:35,901,079**	**T > G**	**0.0022**	**0.84**	**0.0032**	**0.000029**	**110.34**
rs1002399693	**19:35,905,673**	**G > C**	**0.0022**	**0.84**	**0.0031**	**0.00003**	**103.33**

Variants indicated in bold were included in the final haplotype used to identify putative *TYROBP* deletion carriers in the FinnGen data

MAF Minor allele frequency, *NFE* Non-Finnish European

the presence of both variants in the WGS data from three Finnish NHD patients and one monoallelic carrier of the 5.2-kb *TYROBP* deletion, and the rs1244787406 T > G by Sanger sequencing in three NHD patients and four monoallelic carriers (Additional file 1 Fig. S1 A-B). Furthermore, we confirmed the presence of monoallelic *TYROBP* deletion in 49 FinnGen subjects with imputed rs1244787406-G and rs1002399693-C alleles with high (> 0.99) genotype probability. One sample with low genotype probability (0.52) was found to be homozygous for *TYROBP* common variant (Additional file 1 Fig. S1 C). The rs1244787406 T > G was used as the proxy marker for *TYROBP* deletion in all the further analyses conducted in FinnGen data.

We next calculated the frequency by the region of birth for the identified putative *TYROBP* deletion carriers using MAFs for rs1244787406-G in FinnGen. There was no statistically significant difference in the regional distribution (chi-square test, n.s.). The highest frequencies were observed in North Ostrobothnia (MAF = 0.0040) and North Savo (MAF = 0.0036), while the lowest were found in Ostrobothnia (MAF = 0.00063) (Fig. 1C). This regional enrichment is consistent with the previously reported birthplaces of Finnish NHD patients, their parents and grandparents [13, 43]. Together, these results suggest that the rs1244787406-G can be reliably used as a proxy marker to identify carriers of the Finnish founder mutation, the 5.2-kb *TYROBP* deletion.

Monoallelic *TYROBP* deletion associates with an increased risk and earlier onset-age of dementia and AD

To elucidate the phenotypic effect of the monoallelic *TYROBP* deletion, we performed phenome-wide association scan (PheWAS) against 2,489 clinical core endpoints available in FinnGen. PheWAS for rs1244787406-G indicated increased risk of five endpoints related to dementia and Alzheimer's disease (Fig. 2A, Table 2).

To investigate whether the rs1244787406 T > G affects the age of disease onset, we generated Kaplan–Meier survival curves for dementia in general (including AD) (Fig. 2B) and more specifically for AD only (Fig. 2C) illustrating disease free survival from birth to the age at first diagnosis for cases and the age at the end of follow-up for controls. For both dementia and AD, the *TYROBP* deletion proxy marker rs1244787406-G significantly lowered the age at first diagnosis (Fig. 2B-C, Table 3). The effect remained significant when *APOE* ε4 (rs429358) allele was included in the same model (Table 3), suggesting that *TYROBP* increases the risk of AD and dementia independently of *APOE* ε4.

To determine whether the association of *TYROBP* locus with dementia and AD was driven by the

(See figure on next page.)

Fig. 2 Phenotype associations for the *TYROBP* deletion proxy marker rs1244787406-G. **A** Phenotype association study covering 2,489 endpoints indicates significantly increased risk for dementia and AD among carriers of rs1244787406 minor G allele. The dashed line represents genome-wide significance threshold $P = 5 \times 10^{-8}$. **B-C** Kaplan–Meier survival plots showing the proportion free from dementia (B) and AD (C) among rs1244787406-G carriers (purple line) and non-carriers (black line). Shading indicates 95% confidence intervals. X-axis indicates age at the first diagnosis for cases and age at the end of follow-up for controls. **D** Regional association plot of the *TYROBP* locus shows the negative log10-transformed P-values on the y axis for the endpoint 'Dementia (including primary healthcare outpatient registry)' derived from FinnGen. The vertical dashed line represents genome-wide significance threshold $P = 5 \times 10^{-8}$. Each dot represents an individual SNV, and the dot color represents LD with the LD reference variant (purple diamond). The dotted line in the upper panel delineates the area shown in the lower panel. The red vertical lines indicate the 5.2 kb *TYROBP* deletion break points while the shaded grey area represents the *TYROBP* deletion associated shared haplotype region in the lower panel

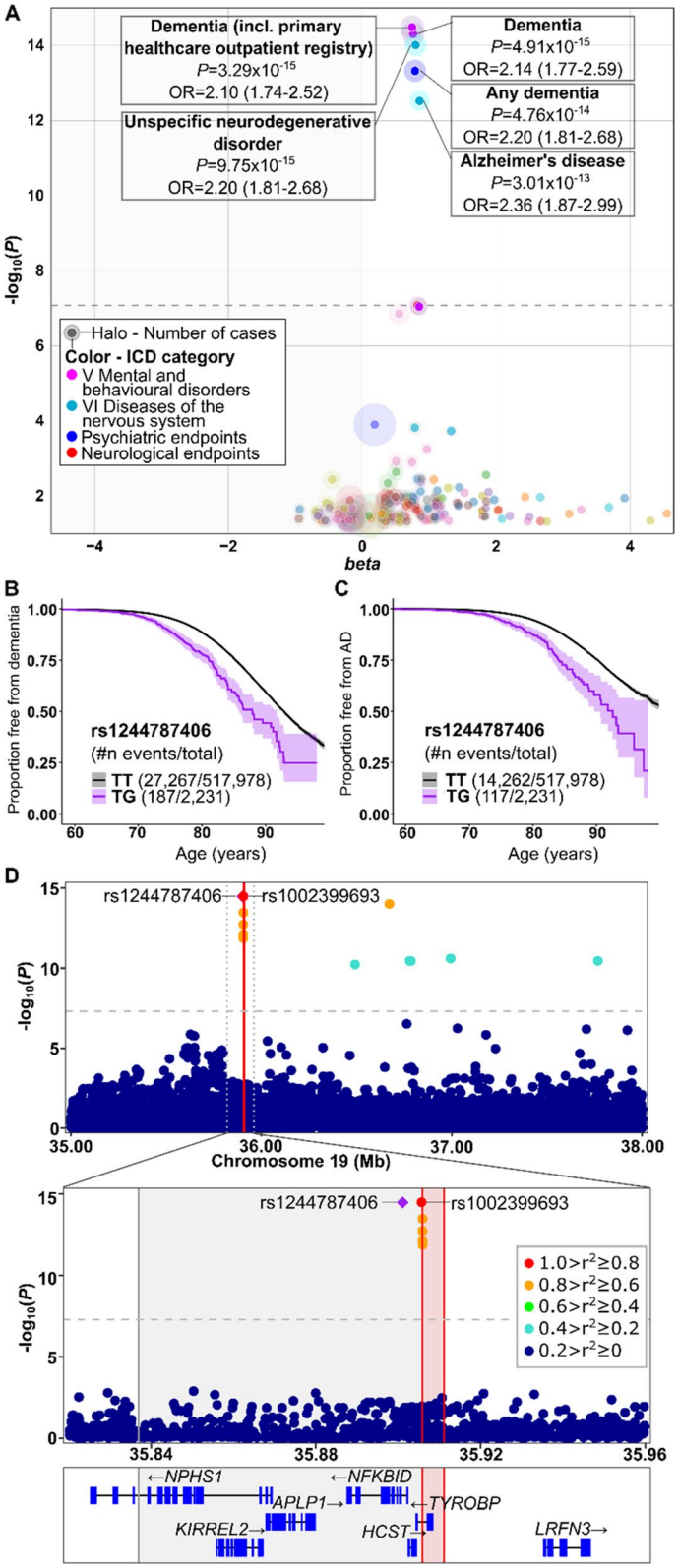

Fig. 2 (See legend on previous page.)

Table 2 Phenotype associations for rs1244787406 (19:35 901 079 T > G) in FinnGen

	OR (95% CI)	P-value	AF case	AF control
Dementia, including primary healthcare outpatient registry	2.10 (1.74–2.52)	3.29e- 15	0.0039	0.0025
Dementia	2.14 (1.77–2.59)	4.91e- 15	0.0039	0.0025
Unspecific neurodegenerative disorder	2.20 (1.81–2.68)	9.75e- 15	0.0042	0.0025
Any dementia	2.20 (1.81–2.68)	4.76e- 14	0.0040	0.0025
Alzheimer's disease	2.36 (1.87–2.99)	3.01e- 13	0.0045	0.0025

AF Allele frequency

Table 3 Hazard ratios for dementia and Alzheimer's disease endpoints in FinnGen cohort

	Dementia, including primary healthcare outpatient registry			Alzheimer		
	HR	95% CI	p-value	HR	95% CI	p-value
rs1442787406	2.14	1.85–2.47	< 2e- 16	2.59	2.16–3.11	< 2e- 16
rs429358	2.30	2.25–2.34	< 2e- 16	2.74	2.67–2.81	< 2e- 16
sex	1.13	1.10–1.16	< 2e- 16	1.07	1.04–1.11	< 2e- 16

The model includes *TYROBP* deletion proxy marker rs1442787406, *APOE* ε4 allele rs429358 and sex

CI Confidence interval, *HR* Hazard ratio

TYROBP deletion proxy markers or other variants in the locus, we produced regional association plots of the *TYROBP* locus (Fig. 2D). The two identified *TYROBP* deletion proxy markers were in high linkage disequilibrium (LD; $r^2 = 1$), had the highest association signal in the locus and were the only significantly associated variants within the known shared *TYROBP* deletion haplotype. Other variants within the *TYROBP* locus were in weaker LD ($r^2 < 0.8$) with the lead variants and were located within the deleted sequence or in the haplotype region shared only by some, but not all *TYROBP* deletion carriers (Fig. 2D, Fig. 1A).

To better understand the role of the variants located within the deleted region detected in FinnGen, we further analyzed our WGS data from three NHD patients and one monoallelic deletion carrier. Variants in the region 19:35,905,884–19:35,905,910 were found to be artefacts arising from the *TYROBP* deletion (Additional file 1 Fig. S2). The deletion breakpoints are located within 120 bp repeated sequence that is almost identical on both sides of the deletion but differs on 15 bases along the repeat. Due to the repeated sequence, reads spanning the deleted area are mapped to one side of the deletion only and the different bases appear as SNVs. However, when large deletions are allowed in the alignment, the reads are aligned correctly and span the deleted sequence, indicating that these SNVs were artefacts arising from the deletion (Additional file 1 Fig. S2).

Monoallelic *TYROBP* deletion induces cystic bone lesions

Bone cysts in the wrists and ankles are an integral feature of NHD caused by the loss of *TYROBP* or *TREM2*. One report has described osteolytic lesions in monoallelic siblings of an NHD patient carrying two different *TYROBP* missense variants [44]. We report here a case of a monoallelic 5.2-kb *TYROBP* deletion carrier with classic painful NHD bone cysts but no detectable brain pathology, cognitive findings, or neuropsychiatric symptoms at age 34 years. Monoallelic 5.2-kb *TYROBP* deletion carrier status was detected in a clinical genetic analysis and confirmed with deletion-specific PCR (Additional file 1 Fig. S1 C). To exclude the possibility of NHD caused by compound heterozygosity, i.e. biallelic state due to the presence of two different NHD-causing variants, WGS analysis was carried out. Only common variants (MAF 0.7–0.71 in the Finnish population according to gnomAD) in *TYROBP* and no variants in *TREM2* were identified in the WGS, confirming that the only NHD-associated variant in the patient was monoallelic 5.2-kb *TYROBP* deletion.

The bone and joint structures of the monoallelic *TYROBP* deletion carrier were otherwise unremarkable, except for two small cystic-appearing translucencies in the wrists (lunates) and slight ulnar minus variance (Fig. 3A), and cystic-appearing translucencies in the left calcaneus and the left distal tibia (Fig. 3B), bearing resemblance to the classical findings in NHD. The carrier's sibling with biallelic *TYROBP* deletion and diagnosed

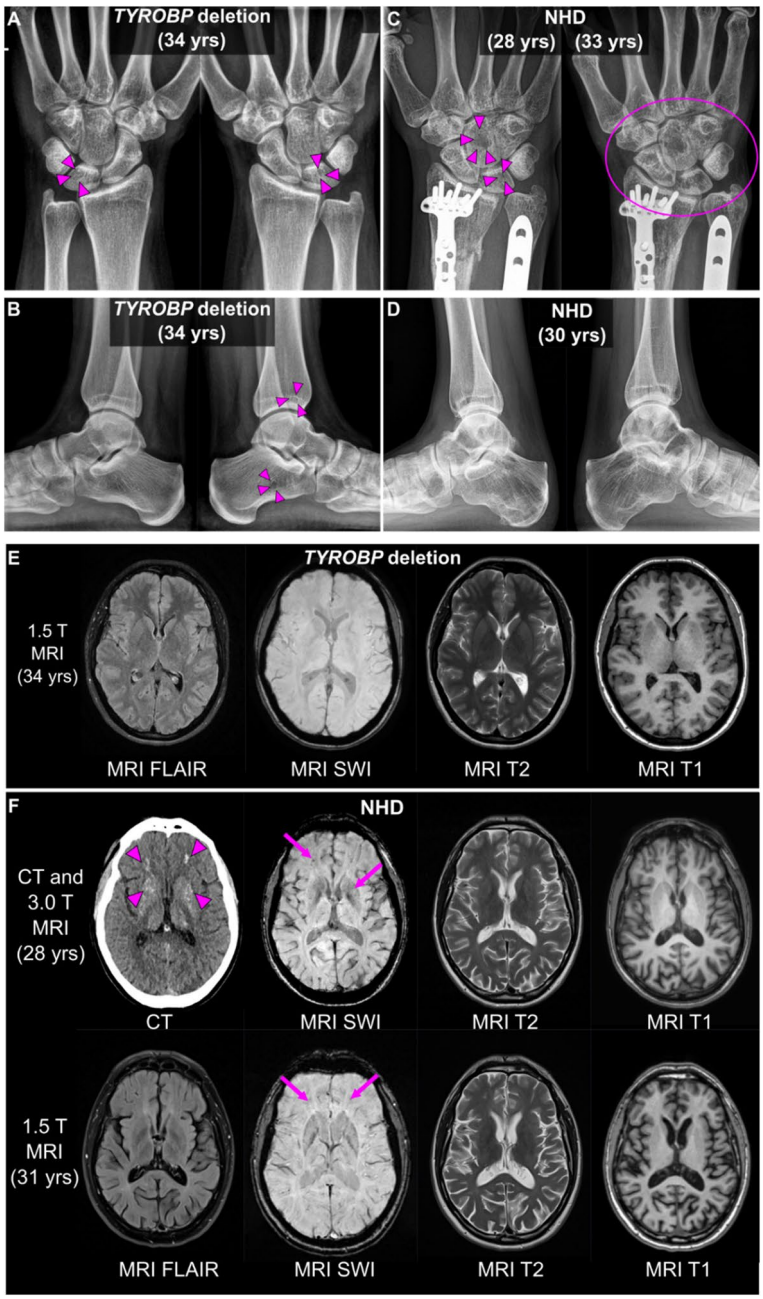

Fig. 3 Clinical imaging of a monoallelic *TYROBP* deletion carrier and an NHD patient. **A-B** Radiographs of wrists and ankles of the monoallelic *TYROBP* deletion carrier show small cystic-appearing translucencies in the lunate bones of the wrists and the left calcaneus and distal tibia of the ankle, as delineated by arrowheads (**C**) Post-traumatic and postoperative radiographs of the NHD patient's right wrist over time span of 5 years. The bone structure is patchy already in the earlier radiograph (on the left), with cystic-appearing translucencies notably in the lunate and capitate. Five years later the primary findings are even more pronounced and all carpal bones as well as the distal radius and ulna present as abnormal (within the ellipse). **D** Radiograph of the NHD patient's ankles shows numerous abnormal translucencies in the distal heads of the tibia and fibula, talar, calcaneal, and cuboid bones. **E** Magnetic resonance images (MRI) of the monoallelic *TYROBP* deletion carrier. No signal or structural pathologies are observable, and there is no evidence of marked atrophy on any of the contrast sets (FLAIR, T1- or T2-weighted, or susceptibility weighted images (SWI)). **F** Computed tomography (CT) and MRI images of the brain of the NHD patient show bilateral calcifications of the basal ganglia and frontal white matter as hyperdensities in the CT scan, denoted by purple arrowheads. Some punctate signal voids can be observed in the corresponding regions on MRI by SWI both at 3.0 T and at 1.5 T field strengths (arrows). FLAIR, T2- or T1-weighted images show no obvious signal pathology. Marked cortical and temporomesial atrophy is however present and shows rapid progression over time

with NHD showed multiple, widespread cystic bone lesions in the hands, wrists, ankles, and feet, with pathological fractures in the right wrist, all consistent with NHD (Fig. 3C-D). No structural or signal pathology was observed on MRI (Fig. 3E) and the brain structural volumes showed no quantitative evidence for atrophic brain pathology in the monoallelic *TYROBP* deletion carrier. The sibling with NHD, however, showed clear findings consistent with NHD: bilateral calcifications of the basal ganglia and frontal white matter, and marked cortical and temporomesial atrophy with rapid progression over time (Fig. 3F). These findings indicate that monoallelic *TYROBP* deletion can cause cystic bone lesions similar to those seen in NHD patients.

Monoallelic *TYROBP* deletion may not affect Aβ pathology in the frontal cortex and CSF

AD-associated variants in *TREM2*, encoding the receptor associated with *TYROBP*, are known to reduce the clustering of microglia around the Aβ plaques [45]. To qualitatively evaluate whether the *TYROBP* loss phenocopies the AD-associated *TREM2* variants, we utilized immunohistochemical staining in frontal cortex biopsies to assess microglial clustering around the Aβ plaques (Fig. 4A) in one monoallelic *TYROBP* deletion carrier and ten non-carriers with different *APOE* genotypes from Kuopio normal pressure hydrocephalus registry, a cohort containing surgical frontal cortex biopsies collected during ventriculoperitoneal shunt placement to treat suspected NPH [16]. In addition, AD-related CSF biomarkers Aβ42, P-Tau181 and total Tau were assessed in the same individuals. There were no major differences in microglial clustering or CSF biomarkers between the *TYROBP* deletion carrier and the non-carriers. The monoallelic *TYROBP* deletion carrier had more plaques per mm^2 of tissue as compared to the non-carriers (Fig. 4B), but Aβ plaque size and microglial clustering around the Aβ plaques were within the same range as in the non-carrier individuals (Fig. 4C-D). Analysis of AD related biomarkers in the CSF indicates significantly decreased Aβ42 levels among the *APOE* ε3ε4 carriers compared to *APOE* ε3ε3 carriers (Fig. 4E) but no differences in the levels of P-Tau181 or total Tau between the genotypes (Additional file 1, Fig. S3 A-D). The CSF biomarker concentrations for the monoallelic *TYROBP* deletion carrier were within the same range as for the other *APOE* ε3ε4 carriers. These findings suggest that the monoallelic *TYROBP* deletion may not have major effects on

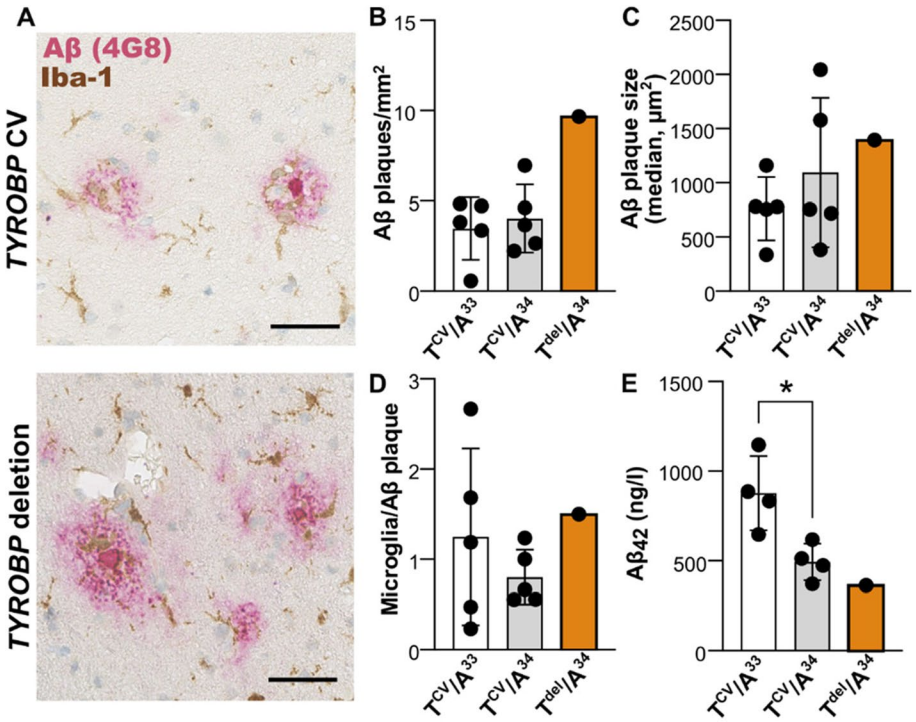

Fig. 4 Effect of the Finnish 5.2-kb TYROBP deletion on AD-related Aβ pathology. **A** A representative image of frontal cortex biopsy immunostained for microglia (Iba- 1, brown) and Aβ (red). Scale bar 50 µm. **B-D** Number (B) and size (**C**) of Aβ plaques, and the number of Aβ plaque-associated microglia (D) in immunohistochemical images shown in (A); n = 1–5 individuals per genotype. **E** Aβ42 levels in the CSF; n = 1–4 individuals per genotype. Data are shown as mean ± SD. Independent samples T-test for T^{CV}/A^{33} and T^{CV}/A^{34}. *: $P < 0.05$. T^{CV}, TYROBP common variant; T^{del}, monoallelic TYROBP deletion; A^{33}, APOE ε3ε3; A^{34}, APOE ε3ε4

AD-related neuropathology. However, a larger number of samples are still needed for the quantitative analyses.

TYROBP deficient monocytes can be differentiated into microglia-like MDMi

To understand the effects of the *TYROBP* deletion in myeloid lineage cells, we obtained monocytes from NHD patients with biallelic *TYROBP* deletion (hereafter referred to as NHD), monoallelic *TYROBP* deletion carriers, and control individuals (Fig. 5A). Since microglia are the primary myeloid cell type in the brain and the only central nervous system resident cell type expressing DAP12 protein derived from *TYROBP*, we next differentiated the monocytes into microglia-like MDMi by culturing the cells for 11–13 days in the presence of M-CSF, GM-CSF, NGF-β, CCL2, and IL- 34, similarly to previous publications [27, 46]. First, we confirmed that the DAP12 protein was robustly expressed in the monocytes and MDMi, and that both the monocytes and MDMi derived from the *TYROBP* deletion carriers displayed reduced DAP12 levels when compared to controls (Fig. 5B). A similar effect was observed at RNA level in both monocytes and MDMi, where the monoallelic *TYROBP* deletion carriers had reduced TYROBP RNA levels as compared to the control individuals carrying the common variant of *TYROBP*, while no TYROBP RNA was detected in cells derived from the NHD patients homozygous for the *TYROBP* deletion (Fig. 5C). These results suggest a gene dose-dependent reduction in *TYROBP*/DAP12 levels in myeloid cells derived from individuals with one or two copies of *TYROBP* deletion compared to individuals with *TYROBP* common variant.

To evaluate the success of microglia-like differentiation, global RNA-sequencing of monocytes and MDMi was carried out (Additional file 2). Furthermore, gene expression profiles of MDMi and monocytes were compared to iPSC and iMGs [28]. PCA analysis indicated that the two microglia-like models, MDMi and iMG, share similar gene expression profiles, distinct from their respective precursor cells, monocytes and iPSC (Fig. 5D). Gene set enrichment analysis (GSEA) further confirmed upregulation of microglial genes (Fig. 5E) and downregulation of monocyte genes (Fig. 5F) in the MDMi. *TREM2*, the key microglial gene and receptor associated with DAP12, was expressed in the MDMi but not in monocytes and was not affected by the *TYROBP* genotype (Fig. 5G). Immunocytochemistry staining revealed a significant expression of the key microglial markers CX3 CR1, IBA1, P2RY12, PU.1, TMEM119, and TREM2 in the MDMi, whereas these markers were not abundantly detected in the monocytes and no unspecific staining was observed in negative controls (Additional file 1, Fig. S4). These results indicate a robust differentiation of the monocytes into microglia-like MDMi cells. Thus, MDMi are a valid model to study the effects of *TYROBP* deletion in microglia-like cells.

TYROBP deletion induces changes in the inflammatory response, unfolded protein response, and cellular metabolic pathways in MDMi cells

To examine the effects of *TYROBP* deletion in microglia-like cells, we carried out differentially expressed gene (DEG) and protein (DEP) analyses in the MDMi cells derived from NHD patients, monoallelic *TYROBP* deletion carriers and individuals homozygous for *TYROBP* common variant. Myelin debris and LPS challenge for 24 h were used to mimic different CNS stress conditions and to activate the TREM2 and TLR4-mediated pathways, respectively. Monoallelic *TYROBP* deletion induced only two DEGs in untreated and myelin-treated conditions when compared to *TYROBP* common variant carriers (Fig. 6A-B, Additional file 3). In contrast, in the LPS-treated condition, several DEGs were observed (Fig. 6C, Additional file 4). A similar trend was observed in the number of differentially expressed proteins (Fig. 6D-F, Additional file 5). Biallelic *TYROBP* deletion had a more robust effect on the gene and protein expression in all conditions when compared to individuals homozygous for the *TYROBP* common variant (Additional file 1 Fig. S5 A-E, Additional file 6) or monoallelic *TYROBP* deletion carriers (Additional file 1 Fig. S6 A-E, Additional file 7). As expected, *TYROBP* was not detected in the NHD MDMi at either the transcript or protein level, whereas a well-established NHD microglial marker CD163 was significantly upregulated at both transcript and protein levels in NHD MDMi when compared to individuals homozygous for *TYROBP* common variant in all comparisons, except in the DEG analysis of untreated cells (Additional file 1 Fig S5).

Gene ontology enrichment was conducted to gain insight into the altered cellular processes induced by mono- or biallelic *TYROBP* deletion. Monoallelic *TYROBP* deletion induced significant upregulation of the inflammatory response, TNFα signaling via NFKB, KRAS signaling up, interferon gamma response, cholesterol homeostasis, apoptosis, and allograft rejection pathways both at the transcript and protein levels upon LPS treatment (Fig. 6G). Simultaneously, a significant downregulation of the unfolded protein response (UPR) and myc targets pathways was observed at both transcript and protein levels (Fig. 6G). Closer inspection of the downregulated pathways revealed, among others, reduced transcript and protein levels of *EIF2 AK3*, which encodes PERK, one of the three sensors of UPR, suggesting that specifically the PERK arm of UPR might be downregulated in monoallelic *TYROBP* deletion

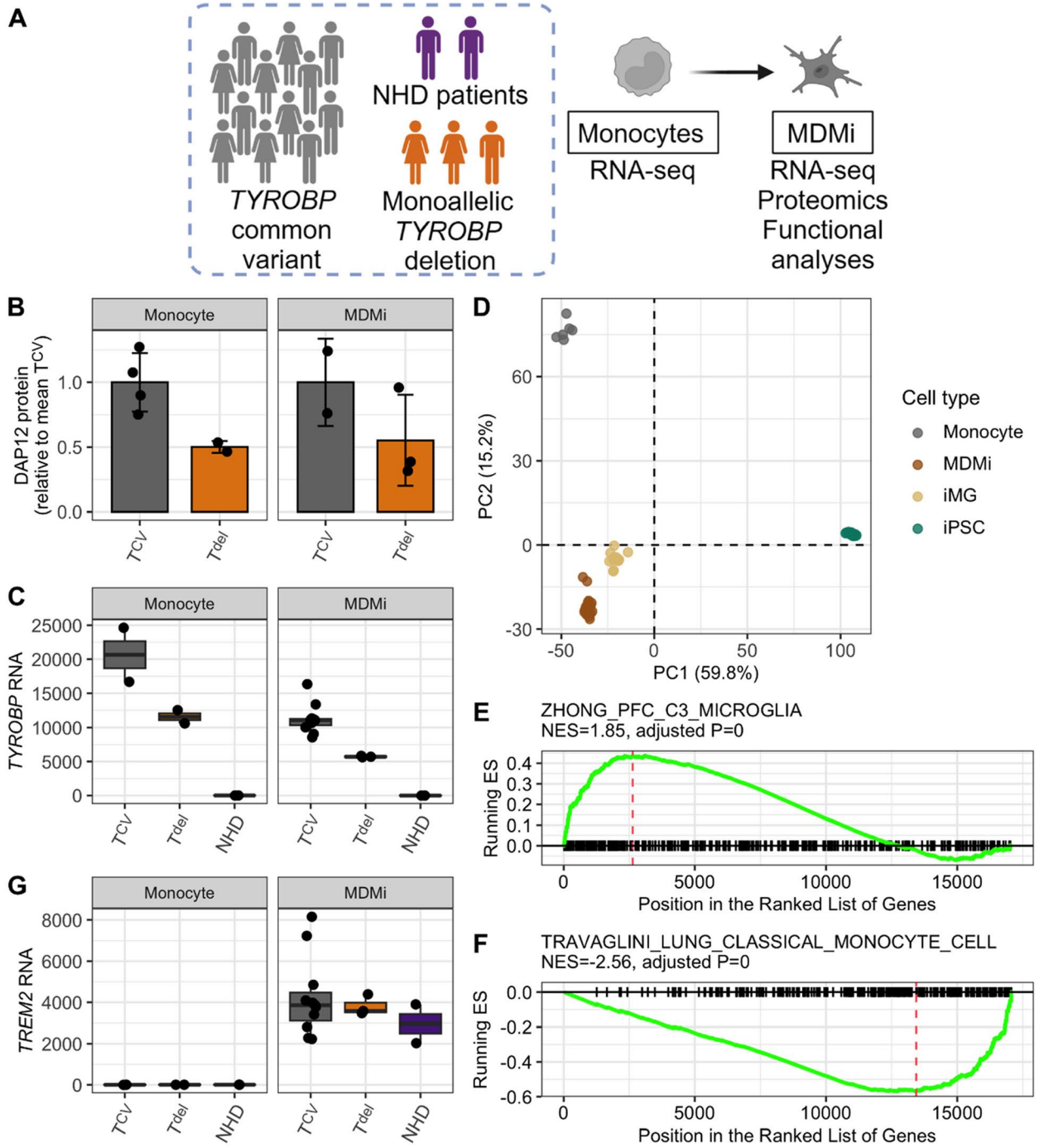

Fig. 5 Characterization of the MDMi cell model. **A** Study design to assess functional effects of the *TYROBP* deletion in MDMi cells. **B** Decreased DAP12 protein levels in the monocytes and MDMi of monoallelic *TYROBP* deletion carriers compared to cells from individuals homozygous for the *TYROBP* common variant. DAP12 protein levels were normalized to GAPDH levels in the same lysate. Monocytes: T^{CV}, n = 4; T^{del}, n = 2; MDMi: T^{CV}, n = 2; T^{del}, *n* = 3. **C** *TYROBP* RNA levels are decreased in monocytes and MDMi of monoallelic *TYROBP* deletion carriers compared to cells from individuals homozygous for *TYROBP* common variant, while no *TYROBP* RNA is detected in NHD patients homozygous for the *TYROBP* deletion. Monocytes: T^{CV}, n = 2; T^{del}, n = 2; NHD, n = 2; MDMi: T^{CV}, n = 8; T^{del}, n = 3; NHD, *n* = 2. **D** Principal component analysis reveals that MDMi and iPSC-derived microglia (iMG) group closely together according to their expression profiles, which were different from their respective precursor cells, monocytes and iPSCs. **E–F** GSEA analysis shows that microglial genes are upregulated (E) while monocyte genes are downregulated (F) in the MDMi cells compared to monocytes. **G** *TREM2* is not expressed in monocytes and is upregulated during MDMi differentiation in all genotype groups. Monocytes: T^{CV}, n = 2; T^{del}, n = 2; NHD, n = 2; MDMi: T^{CV}, n = 8; T^{del}, n = 3; NHD, n = 2. Data in B, C, and G are shown as mean ± SD. Each data point represents one individual

carriers (Fig. 6H). No significant pathway enrichment was observed in untreated, or myelin-treated MDMi from monoallelic *TYROBP* deletion carriers when compared to individuals homozygous for *TYROBP* common variant.

Multiple inflammation related gene sets were upregulated in the NHD compared to *TYROBP* common variant or monoallelic *TYROBP* deletion MDMi, including interferon gamma response, TNFα signaling via NFKB, IL2-STAT5 signaling, and IL6-JAK-STAT3 signaling (Additional file 1 Fig S5 F, S6 F), which were also significantly upregulated in the NHD brain microglia according to a recent single nucleus RNA-sequencing (sn-RNAseq) analysis [47]. Notably, these gene sets were upregulated in the NHD MDMi in all treatment conditions, suggesting a strong proinflammatory transcriptional profile in these cells even without an external stimulus. While the UPR was not among the top downregulated pathways in NHD MDMi when compared to controls, we explored it in more detail to assess potential similarities and differences in MDMi derived from monoallelic *TYROBP* deletion carriers and NHD patients in comparison to controls. Two common downregulated targets, PSAT1 and NPM1, were detected in this pathway (Fig. 6I).

To further validate the inflammatory phenotype induced by *TYROBP* deletion, secretion of IL-6, IL-1β, TNFα, and IL-10 was measured in the conditioned medium collected from the MDMi cells after 24-h LPS stimulation (Fig. 6J-K). IL- 1β secretion was significantly elevated in the MDMi from monoallelic *TYROPB* deletion carriers as compared to control MDMi from individuals homozygous for the *TYROBP* common variant. Even higher increase in IL- 1β secretion was observed in MDMi from a NHD donor. IL- 6 levels did not differ between MDMi from monoallelic *TYROBP* deletion carriers and controls. Over 100-fold increase in secretion of IL- 10 was observed in MDMi from NHD patient compared to other genotypes, in line with the previous snRNA-seq analysis in the brain microglia from NHD patients [47]. TNFα levels did not differ between the genotypes.

Complete *TYROBP* deficiency affects M-CSF-induced signaling

DAP12 encoded by *TYROBP* has a central role in mediating signaling from different cell-surface receptors. To assess how *TYROBP* deletion affects downstream signaling, we generated *Tyrobp* KO BV2 microglial cell lines by lentiviral CRISPR-Cas9 editing (Additional file 1 Fig. S7 A-B). In addition, we used siRNA-mediated *Tyrobp* silencing to mimic cells with monoallelic *TYROBP* deletion (Additional file 1 Fig. S7 A-B). M-CSF is known to induce DAP12-dependent phosphorylation of spleen tyrosine kinase (Syk) in macrophages, osteoclasts, and BV2 microglia [26, 48, 49]. Thus, we stimulated DAP12 deficient and control BV2 cells with M-CSF and assessed the subsequent phosphorylation of Syk as a readout of activation. M-CSF induced a robust increase in the phosphorylation of Syk in control and *Tyrobp* siRNA-treated cells, but not in *Tyrobp* KO cells (Additional file 1 Fig. S7 C). Total Syk levels remained unaltered between control and *Tyrobp* siRNA-treated cells, while approximately 20% reduction in total Syk levels was observed in the *Tyrobp* KO cells (Additional file 1 Fig. S7D). These results indicate that bi- but not monoallelic *Tyrobp* deficiency abolishes the phosphorylation of Syk in response to M-CSF.

Discussion

In this study we show that monoallelic 5.2-kb *TYROBP* deletion is a novel risk factor for AD, leading to two-fold increased risk of AD and dementia with an earlier onset age in the monoallelic carriers when compared to non-carriers. Furthermore, we observed that monoallelic *TYROBP* deletion induces cystic bone lesions typical to NHD caused by biallelic *TYROBP* or *TREM2* loss. The monoallelic *TYROBP* deletion leads to reduced levels of DAP12 protein (encoded by *TYROBP*) in myeloid cells, suggesting that reduction in DAP12 protein levels is the primary mechanism behind these effects, potentially leading to reduced signaling from DAP12-associated receptors. We used microglia-like MDMi derived from peripheral blood monocytes from the carriers to study the effects of *TYROBP* deletion. MDMi express microglial markers and have gene expression signature

(See figure on next page.)

Fig. 6 Increased inflammatory response and decreased unfolded protein response in LPS-treated MDMi cells with *TYROBP* deletion. **A-C** Volcano plots of differentially expressed genes and (**D-F**) proteins in the monoallelic *TYROBP* deletion carrier MDMi cells compared to controls upon untreated (A, D), myelin-treated (B, E) and lipopolysaccharide (LPS)-treated (C, F) conditions., T^{CV}, n = 3–12; T^{del}, n = 3. **(G)** Pathway enrichment of genes (left panel) and proteins (right panel) differentially expressed in the monoallelic *TYROBP* deletion carrier MDMi cells compared to *TYROBP* common variant MDMi cells. **H-I** Heat maps showing the top up- and downregulated targets in the UPR and MYC pathways in the monoallelic (H) and biallelic (I) *TYROBP* deletion carriers compared to controls. **J-K** Inflammatory response was assessed by measuring interleukin-6 (IL-6), IL-1β, IL-10 (J), and tumor necrosis factor α (TNFα; K) levels in the conditioned media of T^{CV}, T^{del}, and NHD MDMi upon 24 h LPS treatment. Each data point indicates one individual, an average of 1–3 replicate wells. T^{CV}, n = 3–4; T^{del}, n = 3–4; NHD, n = 1–2. All data in J are shown as mean ± SD. Independent samples T-test, *: $P < 0.05$. T^{CV}, *TYROBP* common variant; T^{del}, monoallelic *TYROBP* deletion; NHD, Nasu-Hakola disease

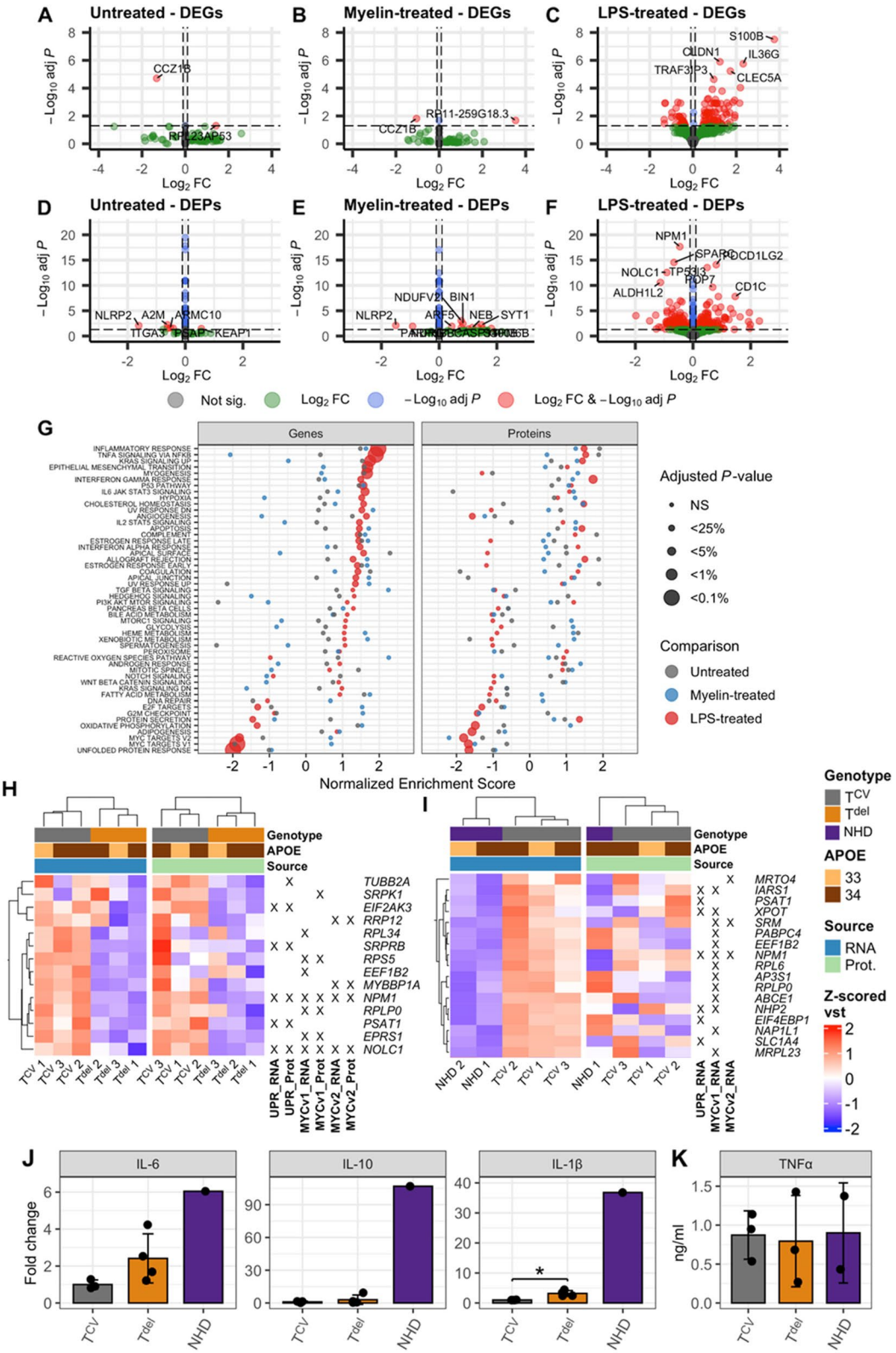

Fig. 6 (See legend on previous page.)

reminiscent of iPSC-derived microglia. Our findings indicate that MDMi derived from monoallelic *TYROBP* deletion carriers display upregulated inflammatory response and downregulated unfolded protein response pathways upon LPS stimulation as compared to control MDMis.

To our knowledge, this is the first report to demonstrate a genetic association at genome-wide significant level between the *TYROBP* locus and AD risk, as well as an earlier onset of dementia and AD. *TYROBP* locus has not been pinpointed in any previous genome-wide association studies for AD, while targeted investigations have led to conflicting results. Enrichment of rare coding variants in *TYROBP* was detected in a cohort of early-onset AD patients [12], while no predicted pathogenic *TYROBP* variants were detected in a cohort of Turkish dementia patients [10]. A previous study among 3,220 older Finns did not detect any association between monoallelic *TYROBP* deletion and cognitive impairment [11]. Due to the rarity of *TYROBP* deletion, only 11 monoallelic carriers were identified in the previous study, potentially limiting its power to detect associations. To overcome this limitation, we utilized FinnGen, the largest available Finnish cohort with genotype and health registry data on 520,210 individuals and detected 2,231 putative monoallelic *TYROBP* deletion carriers using a proxy marker. This approach allowed us to detect increased risk and earlier age of onset for AD and dementia among the monoallelic *TYROBP* deletion carriers compared to non-carriers, which was not dependent on *APOE* status. The previous study reported very low or absent Aβ pathology in the neocortex of two autopsied *TYROBP* deletion carriers [11]. Here, we did not observe differences in Aβ pathology both in the brain tissue and the CSF between single monoallelic *TYROBP* deletion carrier and non-carriers. A higher number of brain tissue and CSF samples should be analyzed to draw definitive conclusions on whether Aβ pathology and the Aβ-associated microglial clustering or CSF biomarkers are affected by monoallelic *TYROBP* deletion.

While earlier genetic evidence has been inconclusive, network based analyses have identified *TYROBP* as a central hub in networks regulating AD pathology and microglial sensory functions [1, 2], highlighting the potential role of *TYROBP* in AD. Paradoxically, studies in mouse models have suggested that partial or complete loss of *Tyrobp* helps to normalize learning behavior deficits and electrophysiological properties associated to cerebral Aβ amyloidosis [50, 51] and tauopathy [52]. Consequently, it has been postulated that reduction of DAP12 levels might present a therapeutic opportunity in AD. This starkly contrasts with our present findings in humans indicating that reduced DAP12 levels caused by monoallelic *TYROBP* loss significantly increase the risk and lower the age of onset of AD. These contradictory findings might arise from species-specific differences [47] or the fact that the AD mouse models cannot fully recapitulate the complexity of the human disease. Nevertheless, they emphasize the importance of human data and humanized models in the search for therapeutic targets in AD.

To begin to understand the functional effects of monoallelic *TYROBP* deletion, we used global transcriptomic and proteomic analyses in a monocyte-derived microglia-like cell model. We found that 24-h LPS stimulation induces upregulation of inflammatory pathways and downregulation of MYC and UPR pathways in the monoallelic *TYROBP* deletion carrier MDMi as compared to MDMi derived from control individuals. Among the top downregulated targets, we highlight PERK (encoded by *EIF2 AK3*). This is one of the three kinases that initiate the UPR signaling. Another identified target was PSAT1, a phosphoserine aminotransferase, whose levels were reduced at both transcript and protein levels in the MDMi from monoallelic *TYROBP* deletion carriers. Intriguingly, emerging results suggest that PERK and PSAT1 converge on metabolic reprogramming that is needed for promoting the immunosuppressive function in M2 macrophages [53] and differentiation of osteoclasts [54]. Specifically, the studies suggest that PERK signaling mediates the upregulation of PSAT1 leading to increased production of α-ketoglutarate, which is an essential cofactor for JMJD3-mediated histone demethylation. This epigenetic mechanism controls genes related to immunosuppression in M2 macrophages and early stages of osteoclastogenesis. Accordingly, this notion unites the two seemingly unconnected pathological processes, bone abnormalities in the monoallelic *TYROBP* deletion carriers and increased immune response in the microglia-like cell model. However, further studies focusing on insults relevant for AD, including Aβ, should be applied in more sophisticated cell models, such as iPSC-derived neuron-microglia co-cultures to better understand the functional effects of monoallelic *TYROBP* deletion.

Cystic bone lesions accompanied by pain, swelling and pathological fractures in the ankles and wrists are the hallmark of the osseous stage of NHD caused by the loss of *TYROBP* or *TREM2* and precede the neurological symptoms. Remarkably, we show that similar cystic-like bone lesions can be detected in the monoallelic carriers of *TYROBP* deletion, corroborating an earlier observation in monoallelic siblings of an Austrian NHD patient carrying different *TYROBP* variants [44]. Intriguingly, genetic silencing or pharmacological inhibition of PSAT1 in mouse osteoclasts leads to an impairment in osteoclast multinucleation [54], similar to that observed in monocyte-derived osteoclasts of NHD patients [55].

Interestingly, some deleterious biallelic *TREM2* variants lead to frontotemporal dementia without bone involvement [6, 7]. Together, this evidence suggests that DAP12 encoded by *TYROBP* may be more critical for the osteoclast function than TREM2.

One of the functions of TREM2-DAP12 pathway in microglia is to promote anti-inflammatory signaling [56]. Thus, the upregulation of immune response pathways observed in monoallelic *TYROBP* deletion carrier and NHD MDMis might be due to the inability of these cells to promote anti-inflammatory signaling. Consequently, these cells may be unable to resolve the immune response once it is activated, similar to the inability of PERK or PSAT1-deficient macrophages to initiate immunosuppressive activity [53]. This was reflected in the increased secretion of proinflammatory IL-1β in both monoallelic *TYROBP* deletion carrier and NHD MDMi as compared to controls. A recent snRNA-seq analysis in *post-mortem* brain of NHD patients observed microglial signature related to tissue repair functions driven by STAT3, RUNX1, and TGFβ [47]. While we did not detect an exactly similar signature in our MDMi cell model, many of the enriched pathways related to immune response are the same in the NHD patient-derived MDMi and the microglia in *post-mortem* NHD brain. In addition to the obvious difference between primary microglia and the microglia-like cell model, these differences may arise because *post-mortem* microglia represent the end stage of the disease, while the MDMi derived from patients in the early neurological stage and cultured in vitro may represent the earlier disease stage.

To study the effects of DAP12 reduction on microglial signaling, we assessed phosphorylation of Syk in response to M-CSF. In line with previous findings in macrophages [48], *Tyrobp* KO BV2 microglial cells were unresponsive to M-CSF stimulation. In contrast, cells with mildly reduced DAP12 levels increased the phosphorylation of Syk similar to control cells. This suggests that complete and partial loss of DAP12 have different effects on the downstream signaling. Thus, further studies are required to fully understand the effect of DAP12 reduction on microglial signaling, particularly in the context of specific ligand-induced TREM2 receptor activation.

Our study has some limitations. We have used an imputed proxy marker to identify *TYROBP* deletion carriers in the FinnGen data since data on large structural variants is not available in FinnGen. It is possible that the use of a proxy marker leads to both inclusion of non-carriers (false positives) and exclusion of true deletion carriers (false negatives). However, we confirmed in a subcohort of 50 individuals from FinnGen by Sanger sequencing that the imputed proxy marker carriers are true 5.2-kb *TYROBP* deletion carriers, except for a rare case of very low imputation Info score, i.e. low quality of the imputed genotype, suggesting that our proxy marker reliably identifies the *TYROBP* deletion carriers. While loss of *TYROBP* expression is the most plausible consequence of the 5.2-kb deletion, we cannot exclude the possibility that the deletion has additional effects besides reduced DAP12 protein levels in myeloid lineage cells demonstrated in our study. While the deleted sequence does not contain any other coding regions besides the exons 1–4 of *TYROBP*, it is possible that the region contains regulatory elements, and their absence might affect the expression of other genes. Replication of our genetic association finding in other populations or additional cohorts is challenging since the 5.2 kb *TYROBP* deletion is a Finnish population specific founder mutation, and our study was conducted using the largest available data release of the unique FinnGen study, combining genotype data and longitudinal health registry data of more than 500,000 individuals, covering approximately 10% of the Finnish population. Other NHD causative *TYROBP* variants are known globally, especially in the Japanese population. However, they are extremely rare, and thus, finding enough monoallelic carriers in a well characterized cohort is unlikely. Nevertheless, our findings are logical due to the close functional connection between DAP12 (encoded by *TYROBP*) and TREM2, and the association of *TREM2* variants with AD risk. While our genetic association finding is robust, a limitation of the study is that we are only beginning to understand the functional effects of the monoallelic *TYROBP* deletion by using a monocyte-derived microglia-like cell model from a small number of donors. However, this is the first report exploring the functional effect of the monoallelic *TYROBP* deletion in microglia-like cells. Our key findings related to altered genes and pathways are supported by both transcriptomic and proteomic analyses. It is well-established that each human in vitro model has its own set of advantages and disadvantages and while iPSC-derived microglia cells better mimic the ontogeny of primary microglia, the monocyte-derived microglia-like cells have been recently used to study the underlying cellular mechanisms linked to genetic alterations in the neurodegenerative diseases [27, 57–60]. In this context, our findings indicated that monocyte-derived microglia-like cells express abundantly a panel of key microglial markers commonly used to validate the identity of in vitro microglial cells, such as CX3 CR1, IBA1, P2RY12, PU.1, TMEM119, and TREM2. Additionally, we compared the bulk RNA-sequencing -based gene expression profile of used monocyte-derived microglia-like cells with the gold-standard microglial cell model, iPSC-derived microglia, and found that these two models share similar gene expression profiles. Importantly, PCA analysis revealed that these two microglia-like models grouped closely together according

to their expression profiles, which were different from their respective precursor cells, monocytes and iPSCs. Although these characterizations support the notion that the monocyte-derived microglia-like cells already provide valuable insights into the cellular mechanisms underlying the monoallelic *TYROBP* deletion, further studies in other relevant human models, such as iPSC-derived microglia-neuron co-cultures are still needed.

Conclusions

In summary, this study identified the monoallelic 5.2-kb *TYROBP* deletion as a novel risk factor which lowers the onset age of AD and dementia, demonstrated for the first time NHD-like bone cysts in a monoallelic *TYROBP* deletion carrier, and provided insights into key biological pathways altered in microglia-like cells due to *TYROBP* deletion.

Abbreviations

AD	Alzheimer's disease
AUC	Area under the curve
CSF	Cerebrospinal fluid
CT	Computed tomography
DEG	Differentially expressed genes
DEP	Differentially expressed proteins
DIA-PASEF	Data Independent Acquisition Parallel Accumulation–Serial Fragmentation
FINGER	Finnish Geriatric Intervention Study to Prevent Cognitive Decline and Disability
iNPH	Idiopathic normal pressure hydrocephalus
KO	Knock-out
LD	Linkage disequilibrium
LFQ	Label-free quantification
LPS	Lipopolysaccharide
MAF	Minor allele frequency
MDMi	Monocyte-derived microglia-like cells
MRI	Magnetic resonance imaging
NHD	Nasu-Hakola disease
PBMC	Peripheral blood mononuclear cell
PheWAS	Phenome-wide association study
PLOSL	Polycystic lipomembranous osteodysplasia with sclerosing encephalopathy
sn-RNAseq	Single-nucleus RNA-sequencing
SNV	Single nucleotide variant
TIMS	Trapped Ion Mobility Spectrometry
TYROBP	TYRO protein tyrosine kinase-binding protein
UPR	Unfolded protein response
WGS	Whole genome sequencing
WT	Wild type

Supplementary Information

The online version contains supplementary material available at https://doi.org/10.1186/s13024-025-00830-3.

Additional file 1

Additional file 2

Additional file 3

Additional file 4

Additional file 5

Additional file 6

Acknowledgements

We are thankful for the NHD patients and their families, and other sample donors for their participation in the study. We acknowledge Research Nurse Tanja Kumpulainen for her valuable work. We acknowledge the Biobank of Eastern Finland and Auria Biobank for access to biobank samples and/or recontacting biobank sample donors. The computational analyzes for WGS, RNA-sequencing, and proteome data were performed on servers provided by UEF Bioinformatics Center, University of Eastern Finland, Finland. Immunohistochemistry and live cell imaging with IncuCyte were carried out using infrastructure of UEF Cell and Tissue Imaging Unit, University of Eastern Finland, Biocenter Kuopio and Biocenter Finland. Illustration in Fig. 5A was created with BioRender.com. We acknowledge the participants and investigators of FinnGen study. Following biobanks are acknowledged for delivering biobank samples to FinnGen: Auria Biobank (www.auria.fi/biopankki), THL Biobank (www.thl.fi/biobank), Helsinki Biobank (www.helsinginbiopankki.fi), Biobank Borealis of Northern Finland (https://www.ppshp.fi/Tutkimus-ja-opetus/Biopankki/Pages/Biobank-Borealis-briefly-in-English.aspx), Finnish Clinical Biobank Tampere (www.tays.fi/en-US/Research_and_development/Finnish_Clinical_Biobank_Tampere), Biobank of Eastern Finland (www.ita-suomenbiopankki.fi/en), Central Finland Biobank (www.ksshp.fi/fi-FI/Potilaalle/Biopankki), Finnish Red Cross Blood Service Biobank (www.veripalvelu.fi/verenluovutus/biopankkitoiminta), Terveystalo Biobank (www.terveystalo.com/fi/Yritystietoa/Terveystalo-Biopankki/Biopankki/) and Arctic Biobank (https://www.oulu.fi/en/university/faculties-and-units/faculty-medicine/northern-finland-birth-cohorts-and-arctic-biobank). All Finnish Biobanks are members of BBMRI.fi infrastructure (www.bbmri.fi). Finnish Biobank Cooperative -FINBB (https://finbb.fi/) is the coordinator of BBMRI-ERIC operations in Finland.

Consortia

FinnGen.

Aarno Palotie, Mark Daly, Bridget Riley-Gills, Howard Jacob, Coralie Viollet, Slavé Petrovski, Chia-Yen Chen, Sally John, George Okafo, Robert Plenge, Joseph Maranville, Mark McCarthy, Rion Pendergrass, Jonathan Davitte, Kirsi Auro, Simonne Longerich, Anders Mälarstig, Anna Vlahiotis, Katherine Klinger, Clement Chatelain, Matthias Gossel, Karol Estrada, Robert Graham, Dawn Waterworth, Chris O´Donnell, Nicole Renaud, Tomi P. Mäkelä, Jaakko Kaprio, Minna Ruddock, Petri Virolainen, Antti Hakanen, Terhi Kilpi, Markus Perola, Jukka Partanen, Taneli Raivio, Jani Tikkanen, Raisa Serpi, Kati Kristiansson, Veli-Matti Kosma, Jari Laukkanen, Marco Hautalahti, Outi Tuovila, Jeffrey Waring, Bridget Riley-Gillis, Fedik Rahimov, Ioanna Tachmazidou, Zhihao Ding, Marc Jung, Hanati Tuoken, Shameek Biswas, Neha Raghavan, Adriana Huertas-Vazquez, Jae-Hoon Sul, Xinli Hu, Åsa Hedman, Ma´en Obeidat, Jonathan Chung, Jonas Zierer, Mari Niemi, Samuli Ripatti, Johanna Schleutker, Mikko Arvas, Olli Carpén, Reetta Hinttala, Johannes Kettunen, Arto Mannermaa, Katriina Aalto-Setälä, Mika Kähönen, Johanna Mäkelä, Reetta Kälviäinen, Valtteri Julkunen, Hilkka Soininen, Anne Remes, Mikko Hiltunen, Jukka Peltola, Minna Raivio, Pentti Tienari, Juha Rinne, Roosa Kallionpää, Juulia Partanen, Adam Ziemann, Nizar Smaoui, Anne Lehtonen, Susan Eaton, Heiko Runz, Sanni Lahdenperä, Natalie Bowers, Edmond Teng, Fanli Xu, Laura Addis, John Eicher, Qingqin S Li, Karen He, Ekaterina Khramtsova, Martti Färkkilä, Jukka Koskela, Sampsa Pikkarainen, Airi Jussila, Katri Kaukinen, Timo Blomster, Mikko Kiviniemi, Markku Voutilainen, Tim Lu, Linda McCarthy, Amy Hart, Meijian Guan, Jason Miller, Kirsi Kalpala, Melissa Miller, Kari Eklund, Antti Palomäki, Pia Isomäki, Laura Pirilä, Oili Kaipiainen-Seppänen, Johanna Huhtakangas, Nina Mars, Apinya Lertratanakul, Marla Hochfeld, Jorge Esparza Gordillo, Fabiana Farias, Nan Bing, Tarja Laitinen, Margit Pelkonen, Paula Kauppi, Hannu Kankaanranta, Terttu Harju, Riitta Lahesmaa, Hubert Chen, Joanna Betts, Rajashree Mishra, Majd Mouded, Debby Ngo, Teemu Niiranen, Felix Vaura, Veikko Salomaa, Kaj Metsärinne, Jenni Aittokallio, Jussi Hernesniemi, Daniel Gordin, Juha Sinisalo, Marja-Riitta Taskinen, Tiinamaija Tuomi, Timo Hiltunen, Amanda Elliott, Mary Pat Reeve, Sanni Ruotsalainen, Dirk Paul, Audrey Chu, Dermot Reilly, Mike Mendelson, Jaakko Parkkinen, Tuomo Meretoja, Heikki Joensuu, Johanna Mattson, Eveliina Salminen, Annika Auranen, Peeter Karihtala, Päivi Auvinen, Klaus Elenius, Esa Pitkänen, Relja Popovic, Margarete Fabre, Jennifer Schutzman, Diptee Kulkarni, Alessandro Porello, Andrey Loboda, Heli Lehtonen, Stefan McDonough, Sauli Vuoti, Kai Kaarniranta, Joni A Turunen, Terhi Ollila, Hannu Uusitalo, Juha Karjalainen, Mengzhen Liu, Stephanie Loomis, Erich Strauss, Hao Chen, Kaisa Tasanen, Laura Huilaja, Katariina Hannula-Jouppi, Teea Salmi, Sirkku Peltonen, Leena Koulu, David Choy, Ying Wu, Pirkko Pussinen, Aino Salminen, Tuula Salo, David Rice, Pekka Nieminen, Ulla Palotie, Maria Siponen, Liisa Suominen,

Päivi Mäntylä, Ulvi Gursoy, Vuokko Anttonen, Kirsi Sipilä, Rion Pendergrass, Hannele Laivuori, Venla Kurra, Laura Kotaniemi-Talonen, Oskari Heikinheimo, Ilkka Kalliala, Lauri Aaltonen, Varpu Jokimaa, Marja Vääräsmäki, Outi Uimari, Laure Morin-Papunen, Maarit Niinimäki, Terhi Piltonen, Katja Kivinen, Elisabeth Widen, Taru Tukiainen, Niko Välimäki, Eija Laakkonen, Jaakko Tyrmi, Heidi Silven, Eeva Sliz, Riikka Arffman, Susanna Savukoski, Triin Laisk, Natalia Pujol, Janet Kumar, Iiris Hovatta, Erkki Isometsä, Hanna Ollila, Jaana Suvisaari, Antti Mäkitie, Argyro Bizaki-Vallaskangas, Sanna Toppila-Salmi, Tytti Willberg, Elmo Saarentaus, Antti Aarnisalo, Elisa Rahikkala, Kristiina Aittomäki, Fredrik Åberg, Mitja Kurki, Aki Havulinna, Juha Mehtonen, Priit Palta, Shabbeer Hassan, Pietro Della Briotta Parolo, Wei Zhou, Mutaamba Maasha, Susanna Lemmelä, Manuel Rivas, Aoxing Liu, Arto Lehisto, Andrea Ganna, Vincent Llorens, Henrike Heyne, Joel Rämö, Rodos Rodosthenous, Satu Strausz, Tuula Palotie, Kimmo Palin, Javier Garcia-Tabuenca, Harri Siirtola, Tuomo Kiiskinen, Jiwoo Lee, Kristin Tsuo, Kati Hyvärinen, Jarmo Ritari, Katri Pylkäs, Minna Karjalainen, Tuomo Mantere, Eeva Kangasniemi, Sami Heikkinen, Nina Pitkänen, Samuel Lessard, Clément Chatelain, Lila Kallio, Tiina Wahlfors, Eero Punkka, Sanna Siltanen, Teijo Kuopio, Anu Jalanko, Huei-Yi Shen, Risto Kajanne, Mervi Aavikko, Helen Cooper, Denise Öller, Rasko Leinonen, Henna Palin, Malla-Maria Linna, Masahiro Kanai, Zhili Zheng, L. Elisa Lahtela, Mari Kaunisto, Elina Kilpeläinen, Timo P. Sipilä, Oluwaseun Alexander Dada, Awaisa Ghazal, Anastasia Kytölä, Rigbe Weldatsadik, Kati Donner, Anu Loukola, Päivi Laiho, Tuuli Sistonen, Essi Kaiharju, Markku Laukkanen, Elina Järvensivu, Sini Lähteenmäki, Lotta Männikkö, Regis Wong, Auli Toivola, Minna Brunfeldt, Hannele Mattsson, Sami Koskelainen, Tero Hiekkalinna, Teemu Paajanen, Shuang Luo, Shanmukha Sampath Padmanabhuni, Marianna Niemi, Javier Gracia-Tabuenca, Mika Helminen, Tiina Luukkaala, Iida Vähätalo, Jyrki Tammerluoto, Sarah Smith, Tom Southerington, Petri Lehto.

Authors' contributions

Conceptualization: HM, MHi Methodology: HM, RMW, MT, PIM Formal analysis: HM, RMW, SH, SAM, TK Investigation: HM, RMW, PH, SAM, MHe, RS, MT, PM, VP, AGR, SPJ, HJ, IK, KS, MN, SVH, MIK, JM, HR, TH, JH, TR Resources: JM, TN, JL, CB, JCL, CH, JR, JH, TR, JK, HS, AH, SFL, VL, ES, MHi Writing – original draft: HM Writing – review & editing: HM, RMW, SH, SAM, MT, SPJ, IK, MN, SVH, MIK, TN, CB, JH, JK, AH, ES, MHi Visualization: HM, SH, RMW Supervision: HM, MHi Project administration: HM Funding acquisition: HM, RMW, MT, HJ, TN, JCL, CH, AH, SFL, VL, ES, MHi All authors reviewed and contributed to the manuscript. The authors read and approved the final manuscript.

Funding

Research Council of Finland, grant 355604 (HM), grant 338182 (MHi), grant 330178 (MT), grant 339767 (VL).
Faculty of Health Sciences, University of Eastern Finland (HM, MT).
Sigrid Jusélius Foundation (MHi, VL, ES, TN).
The Strategic Neuroscience Funding of the University of Eastern Finland (MHi, AH, VL, ES).
Alzheimer's Association ADSF- 24 - 1284326-C (MHi).
ERDF funding for the project "Brain Research Unit 2.0" (MHi)
The State Research Funding KUH-VTR (VL, ES).
Doctoral Programme in Molecular Medicine (RMW, HJ).
Deutsche Forschungsgemeinschaft (DFG, German Research Foundation) under Germany's Excellence Strategy within the framework of the Munich Cluster for Systems Neurology, EXC 2145 SyNergy – ID 390857198 (CH and SFL) and a Koselleck Project HA1737/16 - 1 (CH).
JPco-fuND 2019 Personalised Medicine for Neurodegenerative Diseases; PMG-AD (CH, SFL, JCL, and MHi; local funding agency grant numbers 01ED2002B and 334802).
The FinnGen project is funded by two grants from Business Finland (HUS 4685/31/2016 and UH 4386/31/2016) and the following industry partners: AbbVie Inc., AstraZeneca UK Ltd, Biogen MA Inc., Bristol Myers Squibb (and Celgene Corporation & Celgene International II Sàrl), Genentech Inc., Merck Sharp & Dohme LCC, Pfizer Inc., GlaxoSmithKline Intellectual Property Development Ltd., Sanofi US Services Inc., Maze Therapeutics Inc., Janssen Biotech Inc, Novartis Pharma AG, and Boehringer Ingelheim International GmbH.

Data availability

The datasets supporting the conclusions of this article are included within the article and its additional files. The study participant consent does not allow opening the sequencing (WGS, RNA-seq) or proteomic data generated and analyzed during the current study, but they are available from the corresponding authors (H.M. or M.H.) on a reasonable request. Summary statistics from each FinnGen data release will be made publicly available after a one-year embargo period and can be accessed freely at www.finngen.fi/en/access_results. For individual level data, the Finnish biobank data can be accessed through the Fingenious® services (https://site.fingenious.fi/en/) managed by FINBB. Access to Finnish Health register data can be applied from Findata (https://findata.fi/en/data/).

Declarations

Ethics approval and consent to participate

All study protocols concerning human samples were approved by the Medical Research Ethics Committee of Wellbeing Services County of North Savo (formerly Medical Research Ethics Committee of North Savo Hospital District). Access to biobank samples and participant recontacting were approved by the Scientific Steering Committees of Biobank of Eastern Finland (BB_2020 - 0062, BB23 - 0270) and Auria Biobank (BB_2020 - 0062). Written informed consent was obtained from all participants.
The FinnGen study is approved by Finnish Institute for Health and Welfare (permit numbers: THL/2031/6.02.00/2017, THL/1101/5.05.00/2017, THL/341/6.02.00/2018, THL/2222/6.02.00/2018, THL/283/6.02.00/2019, THL/1721/5.05.00/2019 and THL/1524/5.05.00/2020), Digital and population data service agency (permit numbers: VRK43431/2017–3, VRK/6909/2018–3, VRK/4415/2019–3), the Social Insurance Institution (permit numbers: KELA 58/522/2017, KELA 131/522/2018, KELA 70/522/2019, KELA 98/522/2019, KELA 134/522/2019, KELA 138/522/2019, KELA 2/522/2020, KELA 16/522/2020), Findata (permit numbers THL/2364/14.02/2020, THL/4055/14.06.00/2020, THL/3433/14.06.00/2020, THL/4432/14.06/2020, THL/5189/14.06/2020, THL/5894/14.06.00/2020, THL/6619/14.06.00/2020, THL/209/14.06.00/2021, THL/688/14.06.00/2021, THL/1284/14.06.00/2021, THL/1965/14.06.00/2021, THL/5546/14.02.00/2020, THL/2658/14.06.00/2021, THL/4235/14.06.00/2021), Statistics Finland (permit numbers: TK- 53–1041 - 17 and TK/143/07.03.00/2020 (earlier TK- 53–90 - 20) TK/1735/07.03.00/2021, TK/3112/07.03.00/2021) and Finnish Registry for Kidney Diseases (permission/extract from the meeting minutes on 4th July 2019).
The Biobank Access Decisions for FinnGen samples and data utilized in FinnGen Data Freeze 12 include: THL Biobank BB2017_55, BB2017_111, BB2018_19, BB_2018_34, BB_2018_67, BB2018_71, BB2019_7, BB2019_8, BB2019_26, BB2020_1, BB2021_65, Finnish Red Cross Blood Service Biobank 7.12.2017, Helsinki Biobank HUS/359/2017, HUS/248/2020, HUS/430/2021 §28, §29, HUS/150/2022 §12, §13, §14, §15, §16, §17, §18, §23, §58, §59, HUS/128/2023 §18, Auria Biobank AB17 - 5154 and amendment #1 (August 17 2020), Biobank Borealis of Northern Finland_2017_1013, 2021_5010, 2021_5010 Amendment, 2021_5018, 2021_5018 Amendment, 2021_5015, 2021_5015 Amendment, 2021_5015 Amendment_2, 2021_5023, 2021_5023 Amendment, 2021_5023 Amendment_2, 2021_5017, 2021_5017 Amendment, 2022_6001, 2022_6001 Amendment, 2022_6006 Amendment, 2022_6006 Amendment, 2022_6006 Amendment_2, BB22 - 0067, 2022_0262, 2022_0262 Amendment, Biobank of Eastern Finland 1186/2018 and amendment 22§/2020, 53§/2021, 13§/2022, 14§/2022, 15§/2022, 27§/2022, 28§/2022, 29§/2022, 33§/2022, 35§/2022, 36§/2022, 37§/2022, 39§/2022, 7§/2023, 32§/2023, 33§/2023, 34§/2023, 35§/2023, 36§/2023, 37§/2023, 38§/2023, 39§/2023, 40§/2023, 41§/2023, Finnish Clinical Biobank Tampere MH0004 and amendments (21.02.2020 & 06.10.2020), BB2021 - 0140 8§/2021, 9§/2021, §9/2022, §10/2022, §12/2022, 13§/2022, §20/2022, §21/2022, §22/2022, §23/2022, 28§/2022, 29§/2022, 30§/2022, 31§/2022, 32§/2022, 38§/2022, 40§/2022, 42§/2022, 1§/2023, Central Finland Biobank 1–2017, BB_2021 - 0161, BB_2021 - 0169, BB_2021 - 0179, BB_2021 - 0170, BB_2022 - 0256, BB_2022 - 0262, BB22 - 0067, Decision allowing to continue data processing until 31 st Aug 2024 for projects: BB_2021 - 0179, BB22 - 0067,BB_2022 - 0262, BB_2021 - 0170, BB_2021 - 0164, BB_2021 - 0161, and BB_2021 - 0169, and Terveystalo Biobank STB 2018001 and amendment 25 th Aug 2020, Finnish Hematological Registry and Clinical Biobank decision 18 th June 2021, Arctic biobank P0844: ARC_2021_1001.

Consent for publication

Consent for publication was obtained from participants whose individual data is presented in the manuscript.

Competing interests

CH collaborates with Denali Therapeutics and is a member of the advisory boards of AviadoBio and Cure Ventures. The other authors declare that they have no competing interests.

Author details
[1]Institute of Biomedicine, University of Eastern Finland, Kuopio, Finland. [2]German Center for Neurodegenerative Diseases (DZNE), Munich, Germany. [3]Neuroproteomics, School of Medicine and Health, Technical University of Munich, Munich, Germany. [4]A. I. Virtanen Institute for Molecular Sciences, University of Eastern Finland, Kuopio, Finland. [5]Neuro Center - Neurology, Kuopio University Hospital, Kuopio, Finland. [6]Institute of Clinical Medicine - Neurology, University of Eastern Finland, Kuopio, Finland. [7]Institute for Molecular Medicine Finland (FIMM), Helsinki Institute of Life Science (Hilife), University of Helsinki, Helsinki, Finland. [8]Program in Medical and Population Genetics, Broad Institute of Harvard and MIT, Cambridge, MA, USA. [9]Stanley Center for Psychiatric Research, Broad Institute of Harvard and MIT, Cambridge, MA, USA. [10]Analytic and Translational Genetics Unit, Massachusetts General Hospital, Boston, MA, USA. [11]Department of Clinical Radiology, Imaging Center, Kuopio University Hospital, Kuopio, Finland. [12]Department of Public Health, Finnish Institute for Health and Welfare, Helsinki, Finland. [13]Division of Clinical Geriatrics, Center for Alzheimer Research, Department of Neurobiology, Care Sciences and Society, Karolinska Institutet, Stockholm, Sweden. [14]LabEx DISTALZ - U1167-RID-AGE Facteurs de Risque Et Déterminants Moléculaires Des Maladies Liées Au Vieillissement, Université de Lille, Inserm, CHU Lille, Institut Pasteur de Lille, Lille, France. [15]Metabolic Biochemistry, Faculty of Medicine, Biomedical Centre (BMC), Ludwig-Maximilian University of Munich, Munich, Germany. [16]Munich Cluster for Systems Neurology (Synergy), Munich, Germany. [17]Turku PET Centre, Turku University Hospital, Turku, Finland. [18]InFLAMES Research Flagship Center, University of Turku, Turku, Finland. [19]Unit of Radiology, Institute of Clinical Medicine, University of Eastern Finland, Kuopio, Finland. [20]Department of Clinical Pathology, Kuopio University Hospital, Kuopio, Finland. [21]Unit of Pathology, Institute of Clinical Medicine, University of Eastern Finland, Kuopio, Finland. [22]Research Unit of Clinical Medicine, Neurology, University of Oulu, Oulu, Finland. [23]Medical Research Center, Oulu University Hospital, Oulu, Finland. [24]Neurocenter, Neurology, Oulu University Hospital, Oulu, Finland. [25]Department of Neurosurgery, Kuopio University Hospital, Kuopio, Finland. [26]Institute of Clinical Medicine, University of Eastern Finland, Kuopio, Finland.

Received: 16 May 2024 Accepted: 20 March 2025
Published online: 29 April 2025

References

1. Hickman SE, Kingery ND, Ohsumi TK, Borowsky ML, Wang LC, Means TK, et al. The microglial sensome revealed by direct RNA sequencing. Nat Neurosci. 2013;16(12):1896–905.
2. Zhang B, Gaiteri C, Bodea LG, Wang Z, McElwee J, Podtelezhnikov AA, et al. Integrated systems approach identifies genetic nodes and networks in late-onset Alzheimer's disease. Cell. 2013;153(3):707–20.
3. Paloneva J, Kestilä M, Wu J, Salminen A, Böhling T, Ruotsalainen V, et al. Loss-of-function mutations in TYROBP (DAP12) result in a presenile dementia with bone cysts. Nat Genet. 2000;25(3):357–61.
4. Paloneva J, Manninen T, Christman G, Hovanes K, Mandelin J, Adolfsson R, et al. Mutations in two genes encoding different subunits of a receptor signaling complex result in an identical disease phenotype. Am J Hum Genet. 2002;71(3):656–62.
5. Chouery E, Delague V, Bergougnoux A, Koussa S, Serre JL, Mégarbané A. Mutations in TREM2 lead to pure early-onset dementia without bone cysts. Hum Mutat. 2008;29(9):E194-204.
6. Guerreiro RJ, Lohmann E, Brás JM, Gibbs JR, Rohrer JD, Gurunlian N, et al. Using exome sequencing to reveal mutations in TREM2 presenting as a frontotemporal dementia–like syndrome without bone involvement. JAMA Neurol. 2013;70(1):78–84.
7. Samanci B, Bilgiç B, Gelişin Ö, Tepgeç F, Guven G, Tüfekçioğlu Z, et al. TREM2 variants as a possible cause of frontotemporal dementia with distinct neuroimaging features. Eur J Neurol. 2021;28(8):2603–13.
8. Guerreiro R, Wojtas A, Bras J, Carrasquillo M, Rogaeva E, Majounie E, et al. TREM2 variants in Alzheimer's disease. N Engl J Med. 2013;368(2):117–27.
9. Jonsson T, Stefansson H, Steinberg S, Jonsdottir I, Jonsson PV, Snaedal J, et al. Variant of TREM2 associated with the risk of Alzheimer's disease. N Engl J Med. 2013;368(2):107–16.
10. Darwent L, Carmona S, Lohmann E, Guven G, Kun-Rodrigues C, Bilgic B, et al. Mutations in TYROBP are not a common cause of dementia in a Turkish cohort. Neurobiol Aging. 2017;58:240.e1-240.e3.
11. Kaivola K, Jansson L, Saarentaus E, Kiviharju A, Rantalainen V, Eriksson JG, et al. Heterozygous TYROBP deletion (PLOSLFIN) is not a strong risk factor for cognitive impairment. Neurobiol Aging. 2018;64:159.e1-159.e4.
12. Pottier C, Ravenscroft TA, Brown PH, Finch NA, Baker M, Parsons M, et al. TYROBP genetic variants in early-onset Alzheimer's disease. Neurobiol Aging. 2016;1(48):222.e9-222.e15.
13. Pekkarinen P, Kestilä M, Paloneva J, Terwilliger J, Varilo T, Järvi O, et al. Fine-scale mapping of a novel dementia gene, PLOSL, by linkage disequilibrium. Genomics. 1998;54(2):307–15.
14. Kurki MI, Karjalainen J, Palta P, Sipilä TP, Kristiansson K, Donner KM, et al. FinnGen provides genetic insights from a well-phenotyped isolated population. Nature. 2023;613(7944):508–18.
15. Heyne HO, Karjalainen J, Karczewski KJ, Lemmelä SM, Zhou W, Havulinna AS, et al. Mono- and biallelic variant effects on disease at biobank scale. Nature. 2023;613(7944):519–25.
16. Junkkari A, Luikku AJ, Danner N, Jyrkkänen HK, Rauramaa T, Korhonen VE, et al. The Kuopio idiopathic normal pressure hydrocephalus protocol: initial outcome of 175 patients. Fluids Barriers CNS. 2019;16(1):21.
17. Kivipelto M, Solomon A, Ahtiluoto S, Ngandu T, Lehtisalo J, Antikainen R, et al. The Finnish Geriatric Intervention Study to Prevent Cognitive Impairment and Disability (FINGER): study design and progress. Alzheimers Dement. 2013;9(6):657–65.
18. Ewels PA, Peltzer A, Fillinger S, Patel H, Alneberg J, Wilm A, et al. The nf-core framework for community-curated bioinformatics pipelines. Nat Biotechnol. 2020;38(3):276–8.
19. Dobin A, Davis CA, Schlesinger F, Drenkow J, Zaleski C, Jha S, et al. STAR: ultrafast universal RNA-seq aligner. Bioinformatics. 2013;29(1):15–21.
20. Fauman EB, Keppo S, Cerioli N, Vyas R, Kurki M, Daly M, et al. LAVAA: a lightweight association viewer across ailments. Bioinforma Adv. 2023;3(1):vbad018.
21. Juliusdottir T. topr: an R package for viewing and annotating genetic association results. BMC Bioinformatics. 2023;24(1):268.
22. R Core Team. R: a language and environment for statistical computing. 2023. Available from: https://www.R-project.org.
23. Benner C, Havulinna AS, Järvelin MR, Salomaa V, Ripatti S, Pirinen M. Prospects of fine-mapping trait-associated genomic regions by using summary statistics from genome-wide association studies. Am J Hum Genet. 2017;101(4):539–51.
24. Wang G, Sarkar A, Carbonetto P, Stephens M. A simple new approach to variable selection in regression, with application to genetic fine mapping. J R Stat Soc Ser B Stat Methodol. 2020;82(5):1273–300.
25. Kassambara A, Kosinski M, Biecek P. survminer: drawing survival curves using "ggplot2". 2021. Available from: https://CRAN.R-project.org/package=survminer.
26. Natunen T, Martiskainen H, Marttinen M, Gabbouj S, Koivisto H, Kemppainen S, et al. Diabetic phenotype in mouse and humans reduces the number of microglia around β-amyloid plaques. Mol Neurodegener. 2020;15(1):66.
27. Ryan KJ, White CC, Patel K, Xu J, Olah M, Replogle JM, et al. A human microglia-like cellular model for assessing the effects of neurodegenerative disease gene variants. Sci Transl Med. 2017;9(421):eaai7635.
28. Rostalski H, Hietanen T, Hoffmann D, Heikkinen S, Huber N, Dhingra A, et al. C9orf72 repeat expansion-carrying iPSC-microglia from FTD patients show increased phagocytic activity concomitantly with decreased number of autophagosomal-lysosomal vesicles. bioRxiv; 2024. p. 2024.08.14.607573. Available from: https://www.biorxiv.org/content/10.1101/2024.08.14.607573v1. Cited 2025 Jan 8.
29. Bolger AM, Lohse M, Usadel B. Trimmomatic: a flexible trimmer for Illumina sequence data. Bioinformatics. 2014;30(15):2114–20.
30. Liao Y, Smyth GK, Shi W. The R package Rsubread is easier, faster, cheaper and better for alignment and quantification of RNA sequencing reads. Nucleic Acids Res. 2019;47(8):e47.
31. Love MI, Huber W, Anders S. Moderated estimation of fold change and dispersion for RNA-seq data with DESeq2. Genome Biol. 2014;15(12):550.
32. Zhu A, Ibrahim JG, Love MI. Heavy-tailed prior distributions for sequence count data: removing the noise and preserving large differences. Bioinformatics. 2019;35(12):2084–92.

33. Subramanian A, Tamayo P, Mootha VK, Mukherjee S, Ebert BL, Gillette MA, et al. Gene set enrichment analysis: A knowledge-based approach for interpreting genome-wide expression profiles. Proc Natl Acad Sci. 2005;102(43):15545–50.
34. Liberzon A, Birger C, Thorvaldsdóttir H, Ghandi M, Mesirov JP, Tamayo P. The molecular signatures database hallmark gene set collection. Cell Syst. 2015;1(6):417–25.
35. Hughes CS, Moggridge S, Müller T, Sorensen PH, Morin GB, Krijgsveld J. Single-pot, solid-phase-enhanced sample preparation for proteomics experiments. Nat Protoc. 2019;14(1):68–85.
36. Demichev V, Messner CB, Vernardis SI, Lilley KS, Ralser M. DIA-NN: neural networks and interference correction enable deep proteome coverage in high throughput. Nat Methods. 2020;17(1):41–4.
37. Cox J, Hein MY, Luber CA, Paron I, Nagaraj N, Mann M. Accurate proteome-wide label-free quantification by delayed normalization and maximal peptide ratio extraction, Termed MaxLFQ*. Mol Cell Proteomics. 2014;13(9):2513–26.
38. Larocca JN, Norton WT. Isolation of myelin. Curr Protoc Cell Biol. 2006;33(1):3.25.1-3.25.19.
39. Safaiyan S, Kannaiyan N, Snaidero N, Brioschi S, Biber K, Yona S, et al. Age-related myelin degradation burdens the clearance function of microglia during aging. Nat Neurosci. 2016;19(8):995–8.
40. Therneau T. A package for survival analysis in R. 2024.
41. Therneau TM, Grambsch PM. Modeling survival data: extending the cox model. New York, NY: Springer; 2000. (Dietz K, Gail M, Krickeberg K, Samet J, Tsiatis A, editors. Statistics for Biology and Health). Available from: http://link.springer.com/10.1007/978-1-4757-3294-8. Cited 2024 Feb 29.
42. Chen S, Francioli LC, Goodrich JK, Collins RL, Kanai M, Wang Q, et al. A genomic mutational constraint map using variation in 76,156 human genomes. Nature. 2024;625(7993):92–100.
43. Norio R. The Finnish disease heritage III: the individual diseases. Hum Genet. 2003;112(5):470–526.
44. Shboul M, Roschger P, Ganger R, Paschalis L, Rokidi S, Zandieh S, et al. Bone matrix hypermineralization associated with low bone turnover in a case of Nasu-Hakola disease. Bone. 2019;1(123):48–55.
45. Parhizkar S, Arzberger T, Brendel M, Kleinberger G, Deussing M, Focke C, et al. Loss of TREM2 function increases amyloid seeding but reduces plaque-associated ApoE. Nat Neurosci. 2019;22(2):191–204.
46. Smit T, Ormel PR, Sluijs JA, Hulshof LA, Middeldorp J, de Witte LD, et al. Transcriptomic and functional analysis of Aβ1-42 oligomer-stimulated human monocyte-derived microglia-like cells. Brain Behav Immun. 2022;1(100):219–30.
47. Zhou Y, Tada M, Cai Z, Andhey PS, Swain A, Miller KR, et al. Human early-onset dementia caused by DAP12 deficiency reveals a unique signature of dysregulated microglia. Nat Immunol. 2023;24(3):545–57.
48. Otero K, Turnbull IR, Poliani PL, Vermi W, Cerutti E, Aoshi T, et al. Macrophage colony-stimulating factor induces the proliferation and survival of macrophages via a pathway involving DAP12 and β-catenin. Nat Immunol. 2009;10(7):734–43.
49. Zou W, Reeve JL, Liu Y, Teitelbaum SL, Ross FP. DAP12 couples c-Fms activation to the osteoclast cytoskeleton by recruitment of Syk. Mol Cell. 2008;31(3):422–31.
50. Haure-Mirande JV, Audrain M, Fanutza T, Kim SH, Klein WL, Glabe C, et al. Deficiency of TYROBP, an adapter protein for TREM2 and CR3 receptors, is neuroprotective in a mouse model of early Alzheimer's pathology. Acta Neuropathol (Berl). 2017;134(5):769–88.
51. Haure-Mirande JV, Wang M, Audrain M, Fanutza T, Kim SH, Heja S, et al. Integrative approach to sporadic Alzheimer's disease: deficiency of TYROBP in cerebral Aβ amyloidosis mouse normalizes clinical phenotype and complement subnetwork molecular pathology without reducing Aβ burden. Mol Psychiatry. 2019;24(3):431–46.
52. Audrain M, Haure-Mirande JV, Wang M, Kim SH, Fanutza T, Chakrabarty P, et al. Integrative approach to sporadic Alzheimer's disease: deficiency of TYROBP in a tauopathy mouse model reduces C1q and normalizes clinical phenotype while increasing spread and state of phosphorylation of tau. Mol Psychiatry. 2019;24(9):1383–97.
53. Raines LN, Zhao H, Wang Y, Chen HY, Gallart-Ayala H, Hsueh PC, et al. PERK is a critical metabolic hub for immunosuppressive function in macrophages. Nat Immunol. 2022;23(3):431–45.
54. Stegen S, Moermans K, Stockmans I, Thienpont B, Carmeliet G. The serine synthesis pathway drives osteoclast differentiation through epigenetic regulation of NFATc1 expression. Nat Metab. 2024;6(1):141–52.
55. Paloneva J, Mandelin J, Kiialainen A, Böhling T, Prudlo J, Hakola P, et al. DAP12/TREM2 deficiency results in impaired osteoclast differentiation and osteoporotic features. J Exp Med. 2003;198(4):669–75.
56. Liu W, Taso O, Wang R, Bayram S, Graham AC, Garcia-Reitboeck P, et al. Trem2 promotes anti-inflammatory responses in microglia and is suppressed under pro-inflammatory conditions. Hum Mol Genet. 2020;29(19):3224–48.
57. Xu E, Boddu R, Abdelmotilib HA, Sokratian A, Kelly K, Liu Z, et al. Pathological α-synuclein recruits LRRK2 expressing pro-inflammatory monocytes to the brain. Mol Neurodegener. 2022;17(1):7.
58. Quek H, Cuní-López C, Stewart R, Colletti T, Notaro A, Nguyen TH, et al. ALS monocyte-derived microglia-like cells reveal cytoplasmic TDP-43 accumulation, DNA damage, and cell-specific impairment of phagocytosis associated with disease progression. J Neuroinflammation. 2022;19(1):58.
59. Sellgren CM, Sheridan SD, Gracias J, Xuan D, Fu T, Perlis RH. Patient-specific models of microglia-mediated engulfment of synapses and neural progenitors. Mol Psychiatry. 2017;22(2):170–7.
60. Noh MY, Kwon MS, Oh KW, Nahm M, Park J, Kim YE, et al. Role of NCKAP1 in the defective phagocytic function of microglia-like cells derived from rapidly progressing sporadic ALS. Mol Neurobiol. 2023;60(8):4761–77.

Publisher's Note